Energy efficient information transfer by thalamic relay neurons

Running Title: Energy efficient synaptic transmission

Julia J. Harris[*], Renaud Jolivet[*] and David Attwell

Department of Neuroscience, Physiology & Pharmacology, University College London, Gower St., London, WC1E 6BT, UK

[*] These authors contributed equally to this work.

Correspondence to David Attwell, d.attwell@ucl.ac.uk

Highlights

- How do synapses optimise energy consumption on information transmission?
- We find that increasing synaptic current size increases information transmission.
- But larger or smaller EPSCs decrease the information transmitted per energy used.
- Thus, the biologically observed EPSC size maximises synapse energy efficiency.

Acknowledgements

We thank Sheila Nirenberg for ganglion cell responses to natural visual scenes, Ho Ko for software, Mickey London, Hugh Robinson and Tom Salt for advice, and Guy Billings, Tiago Branco, Matteo Carandini, Lee Cossell, Peter Dayan, Alasdair Gibb, Sonja Hofer, Simon Laughlin, Zhaoping Li, Tom Mrsic-Flogel and Angus Silver for comments. Supported by the European Research Council, Fondation Leducq, MRC, Wellcome Trust and a Marie Curie Fellowship of the EU to R.J. J.J.H. was in UCL's 4 year PhD Programme in Neuroscience.

The architecture of computational devices is shaped by their energy consumption. Energetic constraints are used to design silicon-based computers, but are poorly understood for neural computation. In the brain, most energy is used to reverse the ion influx generating excitatory postsynaptic currents (EPSCs) and action potentials (APs). Thus, postsynaptic currents should be small to minimise energy use, but not so small as to impair information transmission. We quantified information flow through the optic nerve to lateral geniculate nucleus synapse. Altering EPSC size with dynamic clamp, we found that a larger than normal EPSC increases information flow through the synapse. Thus, the biologically-occurring EPSC size does not maximise information flow. By assessing the energy used on postsynaptic ion pumping and action potentials we show that, instead, it optimises the ratio of information transmitted to energy consumed. These data suggest maximisation of information transmission per energy used as a synaptic design principle.

INTRODUCTION

The geometry of excitatory synapses is subject to competing constraints. Synapse diameter needs to be small, firstly so that a neuronal dendrite can receive a large number of synaptic inputs, and secondly because if synapses are too large in diameter then glutamate clearance by diffusion to surrounding astrocytes will be too slow, limiting the maximum rate of information transfer through the synapse (Attwell and Gibb, 2005). On the other hand, if synapses are too small and possess only a few glutamate receptors, then variability in the opening of postsynaptic ion channels creates noise in the postsynaptic signal (Hestrin, 1992; Traynelis et al., 1993). Similarly, since most brain energy is used to pump out ions which enter through postsynaptic receptors (Harris et al., 2012; Howarth et al., 2012), the number of receptors per synapse should be kept small to minimise energy use, but if it is too small the postsynaptic effect of the input will be negligible. How do excitatory synapses cope with these competing requirements?

We employed the optic tract to lateral geniculate nucleus (LGN) synapse to investigate whether the postsynaptic current is large, to transmit as much as possible of the information arriving from the retina, or smaller, to save energy. Surprisingly, increasing the synaptic conductance beyond

the biological norm allows more information flow across the synapse, showing that the synapse properties are not set to maximise information transfer. Instead, analysis of the energetic cost of the postsynaptic ion pumping associated with synaptic signalling (Attwell and Laughlin, 2001) revealed that the synapse properties are set to maximise the information transferred per energy used. In other words, the synapse does not maximise bits transmitted per second, but bits transmitted per ATP molecule.

Theoretical analysis has previously shown that the low mean firing rate of neurons (Levy and Baxter, 1996) and the surprisingly low release probability of central synapses (Harris et al., 2012) can be explained if axons and presynaptic terminals operate to maximise the information transmitted per energy used. The results presented below extend this concept to postsynaptic terminals, the largest consumers of energy in the brain, and suggest that energy use profoundly constrains the operation of the central nervous system.

RESULTS

Spike loss during transmission through the LGN relay synapse

We stimulated optic tract axons making synapses onto whole-cell patch-clamped dorsal LGN relay neurons in the thalamus of rat brain slices (Turner and Salt, 1998) (Figure 1A, Figure S1) with ganglion cell responses to natural visual scenes (Meytlis et al., 2012). The relay neurons were held in tonic firing mode (at -55 mV) as opposed to burst mode (at -70 mV; see Discussion). To isolate a single excitatory input from the optic tract, we used animals at an age (P28) when the retinogeniculate connection is mature (Budisantoso et al., 2012; Chen and Regehr, 2000), cut off the cortex, and blocked $GABA_A$ receptors (Figure 1B, Figure S1; and see Discussion). The stimulus trains used had a mean spike frequency of ~19 Hz, which evoked postsynaptic firing at a mean rate of ~4 Hz (Figure 1C). Thus, despite being designated a "relay synapse", the optic tract to LGN synapse does not ensure an output spike for every input spike. Instead, as first described by Mastronarde (1987), the occurrence of two input action potentials close together in time increases the chance of generating a postsynaptic action potential (Figure 1D).

Spike transmission at this synapse has been observed to vary widely (even within the same species and anaesthetic state: Mastronarde, 1987; Rathbun et al., 2010; Sincich et al., 2009; Usrey et al., 1999; Weyand, 2007), but it is generally agreed that less than 50% of spikes are successfully transmitted (with the average across these papers being 23±8%). We found that only 22% of input action potentials produced an output action potential (Figure 1E-F; and see Experimental Procedures), while 57% produced only an EPSP and 21% produced no detectable EPSP in the following 10 msec (only EPSPs over 1 mV in amplitude were reliably detectable, so this may be an overestimate). Some apparently spontaneous output action potentials were associated with no input stimulus spike in the preceding 10 msec (Figure 1G).

The input action potential train, which was composed of retinal ganglion cell responses to natural movies (from Meytlis et al., 2012) carried 94 bits/sec of information (quantified using the direct method (Strong et al., 1998) but with zero noise entropy). The output spike train recorded in relay neurons carried roughly one fifth of this information (18.3 bits/sec). However, the number of bits of information encoded per action potential was not significantly affected by transmission through the synapse: the input train encoded 4.9 bits/spike (94 bits/sec with a mean firing rate of 19.0 Hz), which is slightly higher than the 1.5-3.5 bits/spike found for natural stimuli in guinea pig retinal ganglion cells (Koch et al., 2006), while on average the output train evoked by synaptic input encoded 4.7 bits/action potential (18.3$\pm$4.5 bits/sec at 3.9$\pm$1.1 Hz), which is similar to a previous report of 3.6 bits/action potential in cat LGN cells (Reinagel and Reid, 2000).

Relationship between synaptic conductance and spike output

How does the reduction in mean spike rate at the LGN synapse affect the amount of information transmitted, and how is information flow affected by the size of the postsynaptic conductance evoked by presynaptic glutamate release? Although not all retinal spikes are transmitted across the synapse, those that are relayed are more informative about the visual stimulus than those that fail to be transmitted (Rathbun et al., 2010; Sincich et al., 2009). Does the relay neuron omit some spikes because they are less informative, or because reliably transmitting them would require a larger EPSC with a correspondingly larger energetic cost? We investigated this by altering the postsynaptic conductance evoked by glutamate release in order to increase or decrease the proportion of retinal

spikes that are transmitted, and examining the effects on information transmission and postsynaptic energy use.

We recorded the sequence of EPSCs evoked by the input action potential train (Figure 2A, B), and examined in current clamp mode the resulting action potential train that these EPSCs generated (Figure 2C). After converting the EPSCs to conductance changes, we used dynamic clamp (Robinson and Kawai, 1993) to inject into the cell soma the recorded conductance scaled up or down by different factors (see Experimental Procedures), so that we could examine the voltage response that would be produced by a larger or smaller synaptic conductance. Figure 2D shows the scaled conductance time course, derived from the current trace in Figure 2B after removal of the stimulus artefact (see Experimental Procedures), for a range of scaling factors. For a synaptic conductance time course injected by dynamic clamp at the soma, with a magnitude equal to that recorded in voltage clamp, the resulting action potential response (Figure 2E) was similar to that evoked by the real synaptic input to the cell (Figure 2C), with a similar mean firing rate (4.2$\pm$1.0 Hz in dynamic clamp; 3.9$\pm$1.1 Hz with synaptic input; 10 cells, not significantly different, $p=0.75$). Scaling the conductance time course evoked by the input signal up or down led to the recorded neuron generating more or fewer spikes, respectively (Figure 2F).

Information transmission

To quantify the information transmitted across the synapse, we measured the mutual information between stimuli and responses using the direct method (Strong et al., 1998; Reinagel and Reid, 2000). Five different spike trains (1-5, Figure 3A) recorded in retinal ganglion cells in response to natural scenes (Meytlis et al., 2012) were used as the stimulus input. Optic tract axons were stimulated with these trains in sequence (1-2-3-4-5), five times (Figure S2A). Each relay neuron therefore responded to each train five times (responses are grouped by input train in Figure 3B). The relay neuron responses to the same input train were generally similar, showing that the output spike trains were not very noisy, while the responses to different trains were very different, showing that the output spike trains had the capacity for high variability, and thus high information content. Mutual information – how much of the input information is transmitted to the output – is the information capacity minus the noise (see Experimental Procedures for full calculations). With presynaptic

stimulation, the mutual information (hereafter simply called "information") was 18.3±4.5 bits/sec (Figure 3C). Employing dynamic clamp to apply the recorded synaptic conductance at the cell soma gave an output information rate of 20.6±4.6 bits/sec, which was not significantly different from that seen with normal synaptic input ($p = 0.59$; Figure 3C).

Energy use on postsynaptic current

We calculated the energy use on the postsynaptic current for each value of the synaptic conductance – either evoked with presynaptic action potentials (Figure 4A-C) or scaled and injected with dynamic clamp (Figure 4D, E) – by calculating the Na^+ entry through the postsynaptic glutamate-gated conductance, and then converting this to ATP use, knowing that one ATP molecule is consumed by the Na^+ pump to extrude 3 Na^+ ions (Attwell and Laughlin, 2001; and see Experimental Procedures). Depolarization of the cell by the postsynaptic current, or by the action potential it evokes, reduces slightly the Na^+ entry through postsynaptic channels compared to the situation in which the cell is voltage-clamped at its resting potential (although this effect is small: Figure 4F). As a result, the energy used on the postsynaptic current increases slightly less than linearly with the effective postsynaptic conductance, although the deviation is small (see Figure 5D, below). Knowing both the information transmitted and the energy used, we could then examine the energetic efficiency of the synapse.

Information transmission and energy efficiency at different synaptic conductances

Examining the output information rate as a function of the postsynaptic conductance (scaled up or down using dynamic clamp) showed that a transmitted information rate 4-fold higher than that observed with the biologically-occurring synaptic conductance magnitude could occur if the postsynaptic conductance was increased (Figure 5A). Increasing the effective synaptic conductance value tended to increase the mean output firing rate (Figure 5B), although in about 30% of cells at large conductance values a depolarizing block (caused by sodium channel inactivation) set in and the firing rate declined again. The information transmitted increased roughly linearly with firing rate, but then reached a plateau (Figure 5C).

The data in Figure 5A demonstrate that the magnitude of the postsynaptic conductance is not set so as to maximise information flow through the synapse, indeed only a small fraction of the input

information is successfully transmitted. Could this apparently sub-optimal arrangement be due to the large energetic cost of synaptic transmission?

We calculated the ratio of the information transmitted through the synapse (Figure 5A) to the energy used on postsynaptic currents (Figure 5D), when dynamic clamp was used to inject synaptic conductances of different magnitude. Strikingly, with either a decrease or an increase of the effective synaptic conductance from its physiological value, the synapse showed a remarkable decrease in energetic efficiency (mean data are shown in Figure 5E but each individual cell showed a similar pattern; see Figures S3 and S4). For example, increasing the synaptic conductance by a factor of 12, which maximises information transmission through the synapse (Figure 5A), more than halved the number of bits of information transmitted per ATP used (Figure 5E). To estimate the position of the peak of the relationship (the optimum), we fitted a curve with the form $100.g_{syn}/g_{opt}$ for $g_{syn}<g_{opt}$, and $100.\exp(-(g_{syn}-g_{opt}))/K$ for $g_{syn}>g_{opt}$, to data from each cell, and varied g_{opt} (and K) to minimise the sum of the squares of the residuals of the fit. The resulting mean value of g_{opt} was 0.90±0.10 (not significantly different from 1, $p = 0.33$). Thus, the optimal value of postsynaptic conductance for maximising the information transmitted per energy used on synaptic currents is not significantly different from the physiologically observed value.

If the postsynaptic current is sufficient to trigger an action potential, an additional energetic cost of restoring ion gradients after the action potential will be incurred. The action potential energy cost per second can be calculated as the product of the cost per action potential ($2.05\pm0.11\times10^7$ ATP molecules for LGN relay neurons; see Experimental Procedures) and the observed firing frequency of the cell (Figure 5B). This cost was added onto the synaptic energy cost that was calculated above, and the information transmitted was calculated relative to the sum of the energy expended on EPSCs and action potentials, as a function of the synaptic conductance scaling factor (Figure 5F). Again, either a decrease or an increase of the synaptic conductance from its physiological value reduced the energetic efficiency of information transmisison (Figure 5F). For each cell, we estimated the position of the peak of the relation in Figure 5F, using the same equation as above. The mean value of g_{opt} was 0.75±0.13 (not significantly different from 1, $p = 0.08$). Thus, the optimal value of postsynaptic

conductance for maximising the information transmitted per energy used on synaptic currents *and* postsynaptic action potentials is again not significantly different from the physiological value.

Effects of local inhibition

In vivo, the retinogeniculate synapse does not act in isolation, but in the presence of GABAergic modulation (both pre- and post-synaptically: Turner and Salt, 1998; Chen and Regehr, 2000; Chen and Regehr, 2003). We therefore performed experiments in the absence of GABAzine, and found that approximately half of patch-clamped relay neurons had observable disynaptic inhibition, which tended to display short-term depression (Figure S1E). Surprisingly, we found that blocking the disynaptic inhibition in these cells by superfusing GABAzine did not alter the firing frequency or information rate when presynaptic stimulation was applied (Figure S1F). Because GABAzine also has no effect on EPSC size (Figure S1F), it appears that local inhibition does not significantly affect the energy efficiency of retinogeniculate transmission.

Modelling the energetic efficiency of the synapse

We used a Hodgkin-Huxley type mathematical model of thalamic relay neurons, with current amplitudes set to those seen experimentally, to check that the membrane currents known to be present in these neurons were sufficient to generate the variation of energetic efficiency with synaptic conductance magnitude which is seen in Figures 5E and F (see Supplemental Information). As shown in Figure S5, this model showed a dependence of information transfer, energy use and energetic efficiency on synaptic conductance that was broadly similar to that measured experimentally in Figure 5, with a peak value of information transmitted per energy used at a synaptic conductance value close to the normal physiological value.

DISCUSSION

We have examined how information flow through a single excitatory synapse is related to the size of the conductance activated by glutamate at the postsynaptic terminal, and hence to the energy expended on postsynaptic ion influx. Strikingly, at the retinal ganglion cell to lateral geniculate nucleus synapse, an increase of postsynaptic conductance (implemented experimentally using dynamic clamp) can increase information flow through the synapse 4-fold (Figure 5A), demonstrating that the synapse properties are far from being optimised to maximise information transmission. Indeed only about 1 in 5 presynaptic action potentials evokes a postsynaptic action potential. However, calculating the energy used on pumping out the Na^+ ions that enter through the postsynaptic conductance (Figure 5E) and during postsynaptic action potentials (Figure 5F) shows that the biologically-observed value of the conductance maximises the ratio of the number of bits of information transmitted through the synapse to the ATP used on ion pumping.

Similar computational sacrifices in favour of energetic efficiency have been observed elsewhere in the brain. The mean firing rate of CNS neurons (~4 Hz: Attwell and Laughlin, 2001; Perge et al., 2009) is much less than the rate that would maximise information coding capacity (about half the maximal firing frequency, or around 200 Hz for a refractory period of 2.5 msec: Levy and Baxter, 1996). This has been explained in terms of neurons maximising the ratio of the amount of information they represent to the energy used on propagating the information as action potentials (Levy and Baxter, 1996). Similarly, the surprisingly low release probability of central synapses has been explained (Harris et al., 2012) in terms of axons and presynaptic terminals operating to maximise the information transmitted per energy used. The results presented here extend this concept to postsynaptic terminals, the largest consumers of energy in the brain. Together with previous results recognizing that energy use is a significant constraint on neuronal function (Attwell and Laughlin, 2001; Perge et al., 2009; Levy and Baxter, 1996; Laughlin and Sejnowski, 2003; Perge et al., 2012; Niven and Farris, 2012), our data suggest maximisation of information transmission per energy used as a design principle of the brain.

Presynaptic optimisation

We did not include in our analysis the energetic costs associated with presynaptic action potentials or presynaptic aspects of synaptic transmission (such as vesicle exo- and endocytosis, glutamate recycling or calcium extrusion) because presynaptic activity is assumed to be fixed by the visual stimulus (and is fixed here experimentally by the natural stimulation patterns used). However, presynaptic release probability may follow a similar optimisation strategy as described in the preceding paragraph.

Tonic and burst modes of thalamic firing

Depending on their resting potential, relay neurons in the thalamus have two modes of firing: tonic mode (at -55 mV), where a single input spike tends to produce (at the most) one output spike, and burst mode (at -70 mV), where a single input spike may produce a burst of output spikes, riding on a depolarising "calcium spike" (Scharfman et al., 1990). Our analysis is restricted to cells firing in the tonic mode seen during alert wakefulness (Coenen and Vendrick, 1972; Livingston and Hubel, 1981). Preliminary data from 3 cells (not shown) suggested that the same optimisation of information transmitted per energy used occurs during burst mode, however the synaptic energy efficiency may differ during less alert states or sleep, when synapses may renormalise their postsynaptic conductances and restore their energy supply (Maret et al., 2011; Vyazovskiy et al., 2008; reviewed in Harris et al., 2012). A complication with carrying out this analysis in burst mode is the uncertainty in how information should be calculated: should bursts be treated as unitary events (in which case, they have been found to carry as much as three times the information of single spikes in tonic mode: Reinagel et al., 1999) or should the spikes within the bursts be treated as independent events, as we have done for tonic mode (in which case, bursts have been reported to contribute negatively to information transfer at the retinogeniculate synapse: Reinagel and Reid, 2000)? A better understanding of which burst features are most relevant to coding at this synapse will be critical to assessing the energetic efficiency of information transmission in burst mode.

Benefits and limitations of isolating a single excitatory synapse

We chose to approach the issue of energy optimisation at the synapse by beginning with the simplest unit: a single, excitatory synapse. The retinogeniculate synapse was an ideal candidate as it

normally receives input from one retinal ganglion cell, and this input can be activated independently of descending excitation from the cortex or local inhibition (Chen and Regehr, 2000). We found that this single synapse performs in an energy efficient way. While energy optimisation principles have been previously demonstrated in the context of single action potentials (Alle et al., 2009; Carter and Bean, 2009; Sengupta et al., 2010), or for the convergence of multiple synapses onto a single postsynaptic cell (Harris et al., 2012), they have never been demonstrated at a single synapse level.

Nevertheless, an important future line of work will be to assess the energetic efficiency of the whole population of retinal synapses onto thalamic neurons. For example, the correlated activity of multiple cells may (Dan et al., 1998), or may not (Meytlis et al., 2012), increase the amount of information available to the visual cortex.

Finally, given our evidence that a single excitatory relay synapse maximises the ratio of information transmitted to energy used, we must ask how general this principle of energy optimisation is across different types of synapses. It seems unlikely that we would have fortuitously come across the only synapse in the brain that is optimised in this way to be energy efficient, but determining whether this is a general rule will require further experimental work. For instance, it will be necessary to examine the energetic efficiency of a synapse which makes a smaller contribution to determining the firing rate of its postsynaptic cell. Minimisation of postsynaptic energy consumption is also likely to be an important constraint on the operation of such synapses, as exemplified by the fact that, after motor learning, approximately 85% of parallel fibre to Purkinje cell synapses are turned off (Isope and Barbour, 2002), greatly reducing the energy consumption of the cerebellar cortex (Howarth et al., 2012). At the other end of the spectrum are synapses like the calyx of Held or neuromuscular junction, where one synaptic input is sufficient to drive a highly reliable postsynaptic response. At such synapses, it may seem that faithful transmission must be favoured at the expense of energy efficiency. However, research at the calyx of Held has shown that, over development, vesicle exocytosis becomes more efficient and release probability decreases, reducing postsynaptic receptor saturation and desensitisation (Taschenberger et al., 2002; Fedchyshyn and Wang, 2005), suggesting that such synapses do not use more resources than are necessary to transmit high fidelity information. We think

it likely that close examination of a variety of synapses will reveal a widespread principle of energy efficient information transmission in the brain.

Potential implications of energy optimisation at the synapse

If the ratio of information transmitted to energy consumed at synapses has to be optimised for normal brain function, this raises the question of whether neurological or psychiatric disorders may arise when this ratio is perturbed. Insertion of too few postsynaptic receptors will lead to an excessive loss of information, while inserting too many postsynaptic receptors could increase the local energetic demand beyond that which can be met by the ATP supply from local mitochondria. To understand how the brain avoids these problems it will be necessary to identify the mechanisms by which neurons assess how well they are optimising information flow in relation to energy consumption. Intriguingly, energy reduction techniques are being introduced to nanoelectronics in which relatively unimportant connections in a semiconductor chip are removed in order to save energy, at the cost of some degradation in the accuracy of the computation performed (Palem and Lingamneni, 2012; Lingamneni et al., 2012). This probabilistic pruning of the circuitry has an effect similar to the sacrifice of information transfer made by neurons that adopt a low postsynaptic conductance in order to save energy.

EXPERIMENTAL PROCEDURES

LGN slice preparation

P28 Sprague Dawley rats were killed by overdose of isoflurane anaesthetic. The brain was rapidly removed and immersed in ice-cold, slicing solution containing (in mM): 87 NaCl, 25 $NaHCO_3$, 7 $MgCl_2$, 2.5 KCl, 1.25 NaH_2PO_4, 0.5 $CaCl_2$, 25 glucose, 75 sucrose, 1 kynurenic acid, saturated with 95% O_2/5% CO_2 (modified from Bischofberger et al., 2006). Parasagittal brain slices containing the dorsal lateral geniculate nucleus (dLGN) were obtained as described in Turner and Salt (1998). Briefly, each hemisphere was isolated using a cut either side of the midline at 3-5° to the sagittal plane, angled outward by 10-25° in the mediolateral plane. The medial side of each brain half was glued to the cutting stage of a vibratome (Leica VT1200S), submerged in ice-cold continuously oxygenated slicing solution and 225 μm slices were made. In general, only a single slice from each hemisphere contained the optic tract and its fibres radiating to the dLGN. Slices were placed in a storage chamber containing continuously oxygenated slicing solution at 35°C, which was allowed to come to room temperature naturally.

Before use, the cortex of each slice was removed using a scalpel to prevent disynaptic excitation via the thalamocortical feedback loop. During the experiment, slices were continuously perfused with artificial cerebrospinal fluid (aCSF) containing (in mM): 124 NaCl, 26 $NaHCO_3$, 10 glucose, 2.5 KCl, 2 $CaCl_2$, 1 NaH_2PO_4, 1 $MgCl_2$, 0.005 GABAzine (to block disynaptic inhibition during stimulation). The aCSF was heated to 35^{o}C and constantly bubbled with 95% O_2/5% CO_2.

Electrophysiology

Whole-cell recordings from relay neurons were obtained using 2-3 MΩ borosilicate glass electrodes filled with the internal solution containing (in mM): 130 K-gluconate, 10 EGTA, 10 HEPES, 4 NaCl, 4 MgATP, 1 $CaCl_2$, 0.5 Na_2GTP, 0.4 K_2-Lucifer yellow. Relay neurons were identified by their large cell bodies (15-25 μm) and the presence of a hyperpolarisation-activated inward current (McCormick and Pape, 1990). Throughout the experiment, relay neurons were held at -55 mV (by injection of a small amount of current, as resting potentials were typically around -70 mV), in order to restrict them to firing in tonic mode (where one input spike generally produces one output spike, as opposed to burst mode at -70 mV, where one input spike generally leads to a burst of

output spike: Scharfman et al., 1990; Reinagel et al., 1999). Online corrections were made for the junction potential of -14 mV for the gluconate-based internal solution used (i.e. neurons were held at an apparent potential of -41 mV to achieve a true potential of -55 mV). Recordings were made with an Axopatch 200B amplifier, filtered at 5 kHz and sampled at 20 kHz. Data were acquired using custom-made MATLAB software, kindly provided by Ho Ko and Tom Mrsic-Flogel, UCL.

The first part of the experiment was performed in voltage clamp. Upon seal formation, pipette capacitance was compensated. Once in whole-cell mode, the series resistance was compensated by up to 70% (after which the mean series resistance was 6.7$\pm$0.6 MΩ). The second part of the experiment was performed in current clamp, using the I-CLAMP FAST mode (which was stable with the 2-3 MΩ pipettes used). In current clamp mode, series resistance compensation was set to 100%.

Retinal ganglion cell axons in the optic tract were stimulated extracellularly with a borosilicate glass electrode (gently broken to achieve a tip diameter of ~10-15 μm) containing aCSF. In voltage clamp, stimulation was adjusted to achieve the minimum reliable EPSC (defined as an EPSC that always occurred and did not vary in size in response to a pulse delivered every 3 s). In most cases, EPSC size increased in one clear step and the stimulus intensity could therefore be set to activate a single presynaptic RGC axon (Budisantoso et al., 2012; Chen and Regehr, 2000) (Figure S1A). This intensity was then maintained throughout the experiment. The average EPSC size (949 ± 141 pA) was similar to that found previously at this age (Budisantoso et al., 2012; Chen and Regehr, 2000) (Figure S1B). All recordings used showed the paired pulse depression characteristic of this synapse (Budisantoso et al., 2012; Chen and Regehr, 2000; Chen et al., 2002) (Figure S1C,D).

Stimulation pattern

RGC axons were stimulated (Figure 1A) with five 5 second spike trains, recorded from ON-RGCs in isolated mouse retinae in response to five natural movies and kindly provided by Sheila Nirenberg, Cornell (Meytlis et al., 2012). After an initial run of Train 3 to habituate the synapse (EPSCs tended to be substantially larger directly after a period of no stimulation), from which the data were discarded, the five trains were played in sequence (1-2-3-4-5), five times, resulting in a 125 sec stimulation train from which data were collected. This procedure was followed once in voltage clamp,

once in current clamp, and several times in dynamic clamp with various conductance gains (see below).

Dynamic clamp

The 125 sec postsynaptic current recording obtained in voltage clamp was used to calculate a 125 sec conductance train. First, the stimulation artefacts were removed by setting the current value for the duration of the artefact to the current value immediately preceding the artefact (Figure 2B inset and 2D inset). The resulting current trace (I_{syn}) was converted to a conductance trace (g_{syn}) via:

$$g_{syn}(t) = I_{syn}(t) / (V_m - V_{rev})$$

where V_m is the membrane potential of the cell (the holding potential, -55 mV), and V_{rev} is the reversal potential of the synapse (0 mV, the reversal potential for glutamatergic ionotropic receptors). g_{syn} was then scaled up or down, by a factor of 0.1, 0.3, 0.5, 0.75, 1, 1.5, 3, 6, 9 or 12. The new 125 sec conductance trace (g_{syn}) was then applied directly to the postsynaptic cell using dynamic clamp (SM-1, Cambridge Conductance: Robinson and Kawai, 1993), which injects a time-varying current $I_{inj}(t)$, at time t, calculated from $g_{syn}(t)$ and the instantaneous value of the cell membrane potential:

$$I_{inj}(t) = g_{syn}(t) \times (V_m(t) - V_{rev})$$

Because of the liquid junction potential, the V_m received by the SM-1 was 14 mV more positive than the real membrane potential. We therefore set V_{rev} on the SM-1 to 14 mV (rather than 0 mV), to account for this in the online calculation of I_{inj}. In this calculation, all of the synaptic current was assumed to scale linearly with membrane potential (i.e. non-linearities related to the magnesium block of NMDA receptors were not mimicked here, but detailed simulations showed that this had no qualitative effect on the relationship between synaptic conductance and the ratio of information transmitted to energy used: Figure S5).

The voltage response of the postsynaptic cell was simultaneously recorded. When the conductance was scaled by 1 and applied by dynamic clamp, the postsynaptic firing pattern was similar to that recorded when electrical stimulation was applied presynaptically (compare Figure 2C and 2E). Thus, although in dynamic clamp the conductance increases were applied at the soma rather than in the dendrites, this did not appear to affect the cell's decision to spike. This was probably because: (1) the conductance injected at the soma was originally recorded at the soma, and was thus

already "filtered" by the dendrites, and may mimic the current injected into the soma from the dendrites during synaptic simulation; and (2) relay neurons in the LGN are highly electrically compact (Bloomfield and Sherman, 1989) which, along with the close proximity of the retinogeniculate synapse to the cell body (< 100 μm: Wilson et al., 1984), implies that the retinal input seen by the soma is only mildly attenuated compared to that seen by the dendrites.

To prevent possible damage to the cell with large injected conductances, the traces scaled by 6, 9 or 12 were always injected last. The order of injection of the smaller conductances was randomised.

Data analysis

Data were analysed using custom scripts written in MATLAB (The Mathworks). Postsynaptic current traces were used to calculate ATP consumption at the synapse as described below. Postsynaptic voltage traces were converted to binarised sequences of 1s (representing action potentials) and 0s (their absence) by identifying events whose amplitude exceeded a threshold defining action potential occurrences (set individually for each cell, between -15 mV and -30 mV). This output sequence could then be compared with the binary input spike train to look at simple transmission characteristics (Figure 1), or used to calculate the amount of information that would be propagated to visual cortex by the postsynaptic cell (Figures 3 and 5).

Synapse transmission characteristics

To assess how the probability of an output spike depends on presynaptic inter-stimulus interval (ISI), output spikes were searched for in the 10 msec following the second spike of an ISI pair. If an output spike was present, the preceding ISI was counted as "relayed", if not, the preceding ISI was counted as "non-relayed". The probability distribution for each category was calculated based on the total frequency counts for all 18 cells studied (Figure 1D). Note that if a single presynaptic spike can sometimes evoke a postsynaptic action potential, this procedure has the potential to artefactually indicate action potential production by large ISIs when in fact it was only the 2^{nd} action potential of a presynaptic pair that produced the postsynaptic action potential; consequently this procedure overestimates the frequency of action potential production by large ISIs.

To assess the occurrence of output responses produced by an input spike, the 10 msec following each input spike was searched for either a 1 in the binarised output trace (indicating a postsynaptic action potential), or an EPSP in the original voltage trace (with a minimum threshold of 1 mV). If neither of these were found, no output response was considered to have occurred. The probability of each outcome was calculated from its relative occurrence across all 18 cells (Figure 1E, F).

To assess the probability of an input spike given an output spike, the 10 msec preceding each output spike was searched for a 1 in the binarised input trace (indicating an input spike). If this was not found, the postsynaptic spike was considered to have occurred spontaneously. The probability of each outcome was calculated from its relative occurrence across all 18 cells (Figure 1E, G).

Calculating synaptic energy use

For voltage clamp conditions, the ATP used to reverse the postsynaptic ion flux (which is the largest synaptic energy cost: Harris et al., 2012) was calculated from the postsynaptic current trace recorded in response to presynaptic stimulation. The current trace was integrated to obtain the total charge entry over the 125 sec recording (Figure 4C). Dividing this by the charge on a Na^+ ion gives an estimate of the Na^+ influx. However, because K^+ efflux is occurring simultaneously (through the non-specific cation pores of AMPA and NMDA receptors), the actual Na^+ entry is 1.42 times larger than this (see next paragraph). The total Na^+ influx must then be actively pumped out by the Na^+/K^+-ATPase, which uses 1 ATP molecule per 3 Na^+ ions. This ATP cost was divided by the length of the recording (125 sec) to get a rate of energy consumption (in ATP molecules/s) for each cell.

For voltage recording in current clamp mode using dynamic clamp, with the synaptic conductance scaled up or down, energy consumption was calculated differently. First, the synaptic Na^+ conductance (g_{Na}) was calculated from the total conductance (g_{syn}) by assuming that the contributions to the total AMPA receptor current carried by Na^+ and K^+ (Ca^{2+} was neglected) vary ohmically with voltage displacement from the reversal potentials V_{Na} (+90 mV) and V_K (-105 mV), so that (for a synaptic current reversal potential of V_{rev}=0 mV),

$$g_{Na} = g_{syn} / (1 - (V_{Na}/ V_K)).$$

For the experimentally imposed reversal potentials stated above, $g_{Na} = (7/13).g_{syn}$. The Na^+ current (I_{Na}) was then calculated directly from the Na^+ conductance, the Na^+ reversal potential, and the membrane potential of the cell as:

$$I_{Na}(t) = g_{Na}(t) \times (V_m(t) - V_{Na}).$$

The integral of $I_{Na}(t)$ was then used to calculate the total postsynaptic Na^+ entry over the 125 sec recording (Figure 4E), which was converted to a rate of energy consumption as above. For voltage-clamp experiments at our holding potential of -55 mV, the Na^+ entry calculated from the equation above can be shown (using the relationship between g_{Na} and g_{syn} given above) to be 1.42-fold larger than the charge entry measured from the synaptic current as $g_{syn}(t) \times (V_m(t)-V_{rev})$.

Calculating action potential energy use

Action potentials in rodent thalamocortical neurons have been found to be highly energy efficient, costing 1.35×10^{11} ATP molecules/AP/cm^2 of membrane (Sengupta et al., 2010). From the recorded membrane capacitance for each cell (mean = 152±8 pF) and the standard biological membrane capacitance (1μF/cm^2), we could calculate the surface area, and thus the action potential cost, for each cell (mean = $2.05 \pm 0.11 \times 10^7$ ATP molecules/AP/cell). This value – calculated for each cell – was multiplied by the firing frequency of the cell in each stimulation condition to obtain the energy used on action potentials per second.

Calculating information

To calculate the information transmitted across the synapse, we assessed the possible repertoire of signal encoding achievable by the optic tract to LGN neuron synapse by applying five separate 5 sec input trains evoked by different natural scenes (Figure 3A). For each recording, we applied these five trains in sequence (1-2-3-4-5), five times (Figure S2A), thus generating a 125 sec output spike train for analysis. We assessed the variability of the output response to the input information (to obtain the "total entropy", calculated below), and also the variability in output response to a single input train applied on five separate occasions (to give the "noise entropy", calculated below).

To calculate the stimulus-related information in the output spike train, we used the direct method (Strong et al., 1998). Binarised output spike trains were binned with 3 msec precision

(approximately the action potential refractory period). The binned trains were examined in segments of a fixed length, called "words" (a particular sequence of 1s and 0s), each word representing a possible neural response. For example, for a word length of five (3 msec) bins, an example word would be 10010. Words were allowed to overlap, so that each time bin was the start of a new word (Dayan and Abbott, 2001; Strong et al., 1998). The action potential string 100100001… would thus yield the 5 letter words 10010, 00100, 01000, 10000, 00001, etc. This maximised the number of words available for analysis in the 125 sec output spike train, the effects of correlations in which are removed by extrapolation to infinite word length (Dayan and Abbott, 2001; Strong et al., 1998) as in Figure S2C. Words that are too long can cause a sampling bias (due to insufficient data being acquired) in which the entropy (calculated below) is underestimated (Dayan and Abbott, 2001; Strong et al., 1998). Choice of word length for the analysis to avoid this problem is discussed below.

A probability distribution of word occurrences was built (Figure S2B), and used to calculate, for two distinct situations (described below), the Shannon entropy (Shannon, 1948), H (in bits), using the general formula:

$$H = -\Sigma\, p(\text{word}) \times \log_2 [p(\text{word})]$$

where p is the probability of a particular word occurring.

First, a probability distribution was built for the occurrence of all possible words of a given length, by counting the frequency of occurrence of each word in the first 25 sec of stimulation (i.e. across the first run of all five trains, represented by the horizontal arrow in Figure S2A). This probability distribution (Figure S2B) was used to calculate the total entropy (H_{total}) of the first 25 sec of the spike train (using the formula above). H_{total} was calculated in this way for each successive run of the five different input trains (i.e. for each row in Figure S2A), and then averaged to get a final estimate of H_{total} for the whole 125 sec recording. H_{total} reflects the maximum possible variability of the postsynaptic response for the input trains used, and a higher value reflects a higher information capacity in the spike train.

Second, to assess variability in the response to a repeated input train (Strong et al., 1998), a probability distribution was built for the occurrence of all possible words (of a given length) that were evoked at a fixed time by a single input train when it was repeated five times. To do this, for a given

word length, and looking at the responses over the 5 repeated identical trains, we counted the frequency of occurrence of words starting at a set time, *t*, after the onset of each repeated train. H_{noise} was calculated in the window from *t* to *t*+(word length) in the repeated train (using the formula above), and then averaged across all time points. H_{noise} was calculated in this way for each different repeated train (i.e. for each column in Figure S2A) and then averaged to get a final estimate of H_{noise} for the whole recording. H_{noise} reflects the trial-to-trial variability of the response, and a lower value reflects low noise levels in the system (i.e. little variability in the response to repeats of the same input).

Subtracting H_{noise} from H_{total} gives an estimate of the mutual information (I, in bits) between the output and input spike trains (Strong et al., 1998), in other words, how informative the output spike train is about the input spike train:

$$I = H_{total} - H_{noise}$$

Because extrapolating to infinite word length (Strong et al., 1998) as in Figure S2C was very computationally time-consuming, we defined the maximum word length that could be used before sampling problems arose by varying the word length between 3 and 63 ms (Figure S2C). We found that total entropy estimates based on 30 msec words differed by only 1.2±0.4% (averaged across dynamic clamp conditions for 3 cells) from the entropy estimate based on a linear extrapolation to infinite word length (Dayan and Abbott, 2001; Strong et al., 1998), while the resulting value of information rate differed by only 0.26±0.57% from the value obtained by extrapolation. Similarly, the relationship between efficiency and g_{syn} was not affected by the use of either extrapolated entropy estimates or entropy estimates based on 30 msec words (or, indeed, words shorter than 30 msec; 3 cells, Figure S3). 30 msec words were therefore used for the entropy calculations that follow. Throughout the paper, entropy and information estimates are divided by the word length (30 msec) to get entropy and information rates in bits/sec.

Data adequacy for entropy calculations

Entropy estimates based on insufficient data could yield misleading results. However, there are significant experimental constraints on the length of whole-cell recordings (applying synaptic stimulation in voltage and current clamp modes, and then applying up to eight different conductance

amplitudes in dynamic clamp takes around one hour and requires exceptional stability of the recorded cell). We therefore used each stimulus train (1-5, Figure 3A) as both a "unique" input (to calculate total entropy) and a "repeat" input (to calculate noise entropy), thus maximising the utility of the data we collect. We checked whether this amount of data was sufficient to produce unbiased entropy estimates by applying the quadratic extrapolation correction described in Strong et al. (1998; their figure 2 inset). Specifically, for every cell's response to presynaptic stimulation, and for one cell's response to every dynamic clamp condition, we fit a quadratic polynomial (Strong et al., 1998) describing how the entropy estimate converges when using increasing fractions of the dataset (Figure S2B inset). The correction (extrapolated value minus value obtained using the whole data set) averaged over the 10 cells for synaptic stimulation was only 1.3 ± 0.4% for the total entropy and 0.6 ± 0.3% for the noise entropy, and averaged over the 7 g_{syn} values in one specimen cell was only 1.0 ± 0.2% for the total entropy and 0.4 ± 0.4% for the noise entropy. We therefore used the empirical values (based on the entire dataset) rather than the quadratically extrapolated values for both total and noise entropies.

For the noise entropy, using 5 repetitions of the same input undersamples the distribution of words for word lengths of 3 bins (9 msec) or longer. Nevertheless, the relationship between synaptic energetic efficiency and g_{syn} was independent of the word length used for the analysis (Figure S3).

Analysis of energetic efficiency

For each condition (real stimulation and all dynamic clamp gains), the information rate was divided by the rate of energy consumption on reversing the ion flux generating EPSCs (Figure 5E), or on reversing the ion flux generating EPSCs and postsynaptic action potentials (Figure 5F), to get a measure of efficiency in bits/(ATP consumed).

Statistics

Data are presented as mean ±s.e.m. Differences between means were assessed with Student's *t*-tests and corrected for multiple comparisons using the Holm-Bonferroni method.

REFERENCES

Alle, H., Roth, A., and Geiger, J.R. (2009). Energy-efficient action potentials in hippocampal mossy fibers. Science *325*, 1405-1408.

Attwell, D., and Gibb, A. (2005). Neuroenergetics and the kinetic design of excitatory synapses. Nat Rev Neurosci *6*, 841-849.

Attwell, D., and Laughlin, S.B. (2001). An energy budget for signaling in the grey matter of the brain. J Cereb Blood Flow Metab *21*, 1133-1145.

Bischofberger, J., Engel, D., Li, L., Geiger, J.R., and Jonas, P. (2006). Patch-clamp recording from mossy fiber terminals in hippocampal slices. Nat Protoc *1*, 2075-2081.

Bloomfield, S.A., and Sherman, S.M. (1989). Dendritic current flow in relay cells and interneurons of the cat's lateral geniculate nucleus. Proc Natl Acad Sci U S A *86*, 3911-3914.

Budisantoso, T., Matsui, K., Kamasawa, N., Fukazawa, Y., and Shigemoto, R. (2012). Mechanisms underlying signal filtering at a multisynapse contact. J Neurosci *32*, 2357-2376.

Carter, B.C., and Bean, B.P. (2009). Sodium entry during action potentials of mammalian neurons: incomplete inactivation and reduced metabolic efficiency in fast-spiking neurons. Neuron *64*, 898-909.

Chen, C., Blitz, D.M., and Regehr, W.G. (2002). Contributions of receptor desensitization and saturation to plasticity at the retinogeniculate synapse. Neuron *33*, 779-788.

Chen, C., and Regehr, W.G. (2000). Developmental remodeling of the retinogeniculate synapse. Neuron *28*, 955-966.

Chen, C., and Regehr, W.G. (2003). Presynaptic modulation of the retinogeniculate synapse. J Neurosci *23*, 3130-3135.

Coenen, A.M., and Vendrik, A.J. (1972). Determination of the transfer ratio of cat's geniculate neurons through quasi-intracellular recordings and the relation with the level of alertness. Exp Brain Res *14*, 227-242.

Dan, Y., Alonso, J.M., Usrey, W.M., and Reid, R.C. (1998). Coding of visual information by precisely correlated spikes in the lateral geniculate nucleus. Nat Neurosci *1*, 501-507.

Dayan, P., and Abbott, L.F. (2001). Theoretical Neuroscience (Cambridge, Massachusetts, The MIT Press).

Fedchyshyn, M.J., and Wang, L.Y. (2005). Developmental transformation of the release modality at the calyx of Held synapse. J Neurosci *25*, 4131-4140.

Harris, J.J., Jolivet, R., and Attwell, D. (2012). Synaptic energy use and supply. Neuron *75*, 762-777.

Hestrin, S. (1992). Activation and desensitization of glutamate-activated channels mediating fast excitatory synaptic currents in the visual cortex. Neuron *9*, 991-999.

Howarth, C., Gleeson, P., and Attwell, D. (2012). Updated energy budgets for neural computation in the neocortex and cerebellum. J Cereb Blood Flow Metab *32*, 1222-1232.

Isope, P., and Barbour, B. (2002). Properties of unitary granule cell-->Purkinje cell synapses in adult rat cerebellar slices. J Neurosci *22*, 9668-9678.

Koch, K., McLean, J., Segev, R., Freed, M.A., Berry, M.J., 2nd, Balasubramanian, V., and Sterling, P. (2006). How much the eye tells the brain. Curr Biol *16*, 1428-1434.

Laughlin, S.B., and Sejnowski, T.J. (2003). Communication in neuronal networks. Science *301*, 1870-1874.

Levy, W.B., and Baxter, R.A. (1996). Energy efficient neural codes. Neural Comput *8*, 531-543.

Lingamneni, A., Muntimadugu, K.K., Enz, C., Karp, R.M., Palem, K.V., and Piguet, C. (2012). Algorithmic methodologies for ultra-efficient inexact architectures for sustaining technology scaling. Proc 9th ACM Int Conf on Computing Frontiers 3-12.

Livingstone, M.S., and Hubel, D.H. (1981). Effects of sleep and arousal on the processing of visual information in the cat. Nature *291*, 554-561.

Maret, S., Faraguna, U., Nelson, A.B., Cirelli, C., and Tononi, G. (2011). Sleep and waking modulate spine turnover in the adolescent mouse cortex. Nat Neurosci *14*, 1418-1420.

Mastronarde, D.N. (1987). Two classes of single-input X-cells in cat lateral geniculate nucleus. II. Retinal inputs and the generation of receptive-field properties. J Neurophysiol *57*, 381-413.

McCormick, D.A., and Pape, H.C. (1990). Properties of a hyperpolarization-activated cation current and its role in rhythmic oscillation in thalamic relay neurones. J Physiol *431*, 291-318.

Meytlis, M., Nichols, Z., and Nirenberg, S. (2012). Determining the role of correlated firing in large populations of neurons using white noise and natural scene stimuli. Vision Res *70*, 44-53.

Niven, J.E., and Farris, S.M. (2012). Miniaturization of nervous systems and neurons. Curr Biol *22*, R323-329.

Palem, K., and Lingamneni, A. (2012). What to do about the end of Moore's law, probably! . Proc 49th Ann Design Automation Conf, 924-929.

Perge, J.A., Koch, K., Miller, R., Sterling, P., and Balasubramanian, V. (2009). How the optic nerve allocates space, energy capacity, and information. J Neurosci *29*, 7917-7928.

Perge, J.A., Niven, J.E., Mugnaini, E., Balasubramanian, V., and Sterling, P. (2012). Why do axons differ in caliber? J Neurosci *32*, 626-638.

Rathbun, D.L., Warland, D.K., and Usrey, W.M. (2010). Spike timing and information transmission at retinogeniculate synapses. J Neurosci *30*, 13558-13566.

Reinagel, P., Godwin, D., Sherman, S.M., and Koch, C. (1999). Encoding of visual information by LGN bursts. J Neurophysiol *81*, 2558-2569.

Reinagel, P., and Reid, R.C. (2000). Temporal coding of visual information in the thalamus. J Neurosci *20*, 5392-5400.

Robinson, H.P., and Kawai, N. (1993). Injection of digitally synthesized synaptic conductance transients to measure the integrative properties of neurons. J Neurosci Methods *49*, 157-165.

Scharfman, H.E., Lu, S.M., Guido, W., Adams, P.R., and Sherman, S.M. (1990). N-methyl-D-aspartate receptors contribute to excitatory postsynaptic potentials of cat lateral geniculate neurons recorded in thalamic slices. Proc Natl Acad Sci U S A *87*, 4548-4552.

Sengupta, B., Stemmler, M., Laughlin, S.B., and Niven, J.E. (2010). Action potential energy efficiency varies among neuron types in vertebrates and invertebrates. PLoS Comput Biol *6*, e1000840.

Shannon, C.E. (1948). A mathematical theory of communication. Bell System Tech J *27*, 379-423.

Sincich, L.C., Horton, J.C., and Sharpee, T.O. (2009). Preserving information in neural transmission. J Neurosci *29*, 6207-6216.

Strong, S.P., Koberle, R., de Ruyter van Steveninck, R., and Bialek, W. (1998). Entropy and Information in Neural Spike Trains. Phys Rev Lett *80*, 197-200.

Taschenberger, H., Leao, R.M., Rowland, K.C., Spirou, G.A., and von Gersdorff, H. (2002). Optimizing synaptic architecture and efficiency for high-frequency transmission. Neuron *36*, 1127-1143.

Traynelis, S.F., Silver, R.A., and Cull-Candy, S.G. (1993). Estimated conductance of glutamate receptor channels activated during EPSCs at the cerebellar mossy fiber-granule cell synapse. Neuron *11*, 279-289.

Turner, J.P., and Salt, T.E. (1998). Characterization of sensory and corticothalamic excitatory inputs to rat thalamocortical neurones in vitro. J Physiol *510 (Pt 3)*, 829-843.

Usrey, W.M., Reppas, J.B., and Reid, R.C. (1999). Specificity and strength of retinogeniculate connections. J Neurophysiol *82*, 3527-3540.

Vyazovskiy, V.V., Cirelli, C., Pfister-Genskow, M., Faraguna, U., and Tononi, G. (2008). Molecular and electrophysiological evidence for net synaptic potentiation in wake and depression in sleep. Nat Neurosci *11*, 200-208.

Weyand, T.G. (2007). Retinogeniculate transmission in wakefulness. J Neurophysiol *98*, 769-785.

Wilson, J.R., Friedlander, M.J., and Sherman, S.M. (1984). Fine structural morphology of identified X- and Y-cells in the cat's lateral geniculate nucleus. Proc R Soc Lond B Biol Sci *221*, 411-436.

FIGURE LEGENDS

Figure 1. Spike transmission through the optic tract–LGN synapse. (A) Slice preparation showing the stimulating electrode in the optic tract and the recording electrode in the dorsal LGN. (B) Circuitry of the LGN with functioning pathways in black (axons from the retina and to the visual cortex) and inactivated pathways in grey (cortex is removed to remove cortical input, and inhibition from interneurons is abolished with GABAzine). (C) Spike frequency in the input stimulus train (Input) and evoked in 18 LGN cells (Output). (D) Probability of an output action potential (AP) as a function of interstimulus interval between 2 preceding presynaptic APs. (E) Logical table stating possible input and output combinations, with specimen examples of each. (F) Observed outcomes given an input AP (EPSPs had to be larger than 1 mV to be counted). (G) Observed input APs given an output AP.

Figure 2. Conversion of synaptic conductance to action potentials. (A) A section of the stimulus train applied to the optic tract axon. (B) The EPSC train evoked in the LGN cell by the input train when voltage-clamped at -55 mV. (C) The AP sequence evoked in current clamp mode by the train in A. Large vertical deflections in B (grey in inset) and small downward deflections in C are stimulus artefacts. (D) The EPSC conductance time course derived from B for injection by dynamic clamp, with the same amplitude as evoked by synaptic input (g x 1) and scaled up and down in size (g x 3, g x ½). (E) AP stream evoked by dynamic clamp injection at the soma of the g x 1 conductance trace in D. (F) AP stream evoked by dynamic clamp injection of the g x 3 and g x ½ conductance traces in D. All data from same cell.

Figure 3. Information conveyed to the LGN by natural scenes. (A) Five second segments of AP streams (1-5) recorded from ganglion cell axons in response to natural scenes (Meytlis et al., 2012). (B) AP responses (each line is one AP) of a specimen cell to 5 separate applications of trains 1-5 to the optic tract (real stimulation). (C) Output information in 10 cells when the cell received AP evoked synaptic currents (real stimulation) or had the measured conductance evoked by real stimulation injected at the soma with the same magnitude (dynamic clamp x1).

Figure 4. Energy use on postsynaptic currents. (A) Two stimuli from one of the stimulus trains, chosen to evoke (B) an action potential or just an EPSC. (C) The EPSCs evoked by the stimuli recorded at -55 mV in voltage-clamp. The action potential in response to the first stimulus (as shown in B) requires a larger EPSC (note that, because current was recorded in voltage-clamp mode, it does not reflect the sodium influx associated with the action potential itself). Integrating the current trace (area shaded in grey) gives the total postsynaptic charge entry. The actual Na^+ entry is 1.42 times larger than this (see Experimental Procedures). Na^+ entry is then converted to ATP cost at a rate of 1 ATP molecule per 3 Na^+ ions. (D) The synaptic current, calculated from the conductance derived from C, that is injected in dynamic clamp (with conductance scaling factor of 1). Since the membrane potential is not voltage-clamped, the current shows an outward deflection as the action potential depolarizes the cell positive to the reversal potential for the synapse. (E) The Na^+ current calculated to occur during dynamic clamping. (F) The ATP used on extruding Na^+ entering through the postsynaptic conductance, calculated under voltage-clamp conditions during stimulation of the optic tract, and when injecting the same conductance at the soma using dynamic clamp (10 cells).

Figure 5. Postsynaptic conductance magnitude maximises information transferred per energy used. (A) Dependence of the output information on synaptic conductance (g_{syn}) magnitude, when cells were stimulated with dynamic clamp (black points) with g_{syn} x1 (applied to all 10 cells) and other values (6 cells for g_{syn} x0.1, 7 cells for x0.3, 9 cells for x0.5, 3 cells for x0.75, 3 cells for x1.5, 8 cells for x3, 7 cells for x6, 7 cells for x9, 4 cells for x12), or with optic tract stimulation (blue point, 10 cells). Information is normalised to the value with g_{syn} x1 for which the mean information rate was 20.6$\pm$4.6 bits/sec. Colours and number of cells per condition are the same in A and D-F. (B) Relationship between firing frequency and g_{syn} for 10 cells (fitted equation has the form $F_{max}.g_{syn}^{n}/(g_{syn}^{n}+g_{syn0.5}^{n})$, where F_{max}=9.9 Hz, n=2, $g_{syn0.5}$=1.4). (C) Dependence of output information on mean output firing frequency evoked by stimulus trains with different g_{syn} values in 10 cells (fitted equation has the form $I_{max}.(1-\exp(-af^{n})$, where I_{max}=83 bits/sec, a=0.1, n=1.2 and f is frequency). (D) Energy use on pumping out of postsynaptic ion influx as a function of g_{syn} multiplier used in dynamic clamp. (E) Output information divided by energy use on reversing the ion influx generating

postsynaptic currents in 10 cells shows a maximum at the physiological value of g_{syn}. 100% corresponds to 15.6±2.7 bits per 10^8 ATP molecules used. Equation fitted to all the data has the form $100.g_{syn}/g_{opt}$ for $g_{syn}<g_{opt}$, and $100.\exp(-(g_{syn}-g_{opt}))/K$ for $g_{syn}>g_{opt}$, where $g_{opt}=0.91$ and $K=9.36$. (F) Output information divided by energy use on reversing the ion influx generating postsynaptic currents and postsynaptic action potentials also shows a maximum at the physiological value of g_{syn}. 100% corresponds to 9.0±1.2 bits per 10^8 ATP molecules used. Fitted equation as in D, but with $g_{opt}=0.78$ and $K=9.95$.

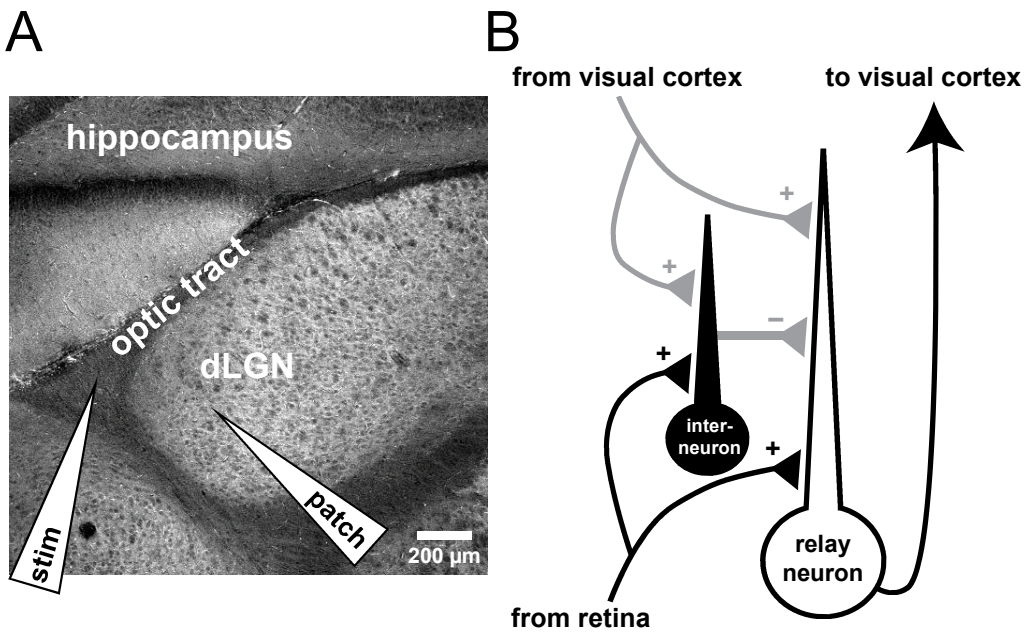
A
hippocampus
optic tract
dLGN
stim
patch
200 µm
B
from visual cortex
to visual cortex
inter-
neuron
relay
neuron
from retina
C
Spike frequency (Hz)
20
16
12
8
4
0
Input
Output
D
Probability
.12
.10
.08
.06
.04
.02
0
followed by output AP
not followed by output AP
0
10
20
30
40
50
ISI (ms)
E
Input
Output
Example
1
0
2 mV
2.5 ms
1
EPSP
2 mV
2.5 ms
1
AP
10 mV
2.5 ms
0
AP
10 mV
2.5 ms
F
22%
21%
57%
Output given input AP
G
21%
79%
Input given output AP

Figure 1

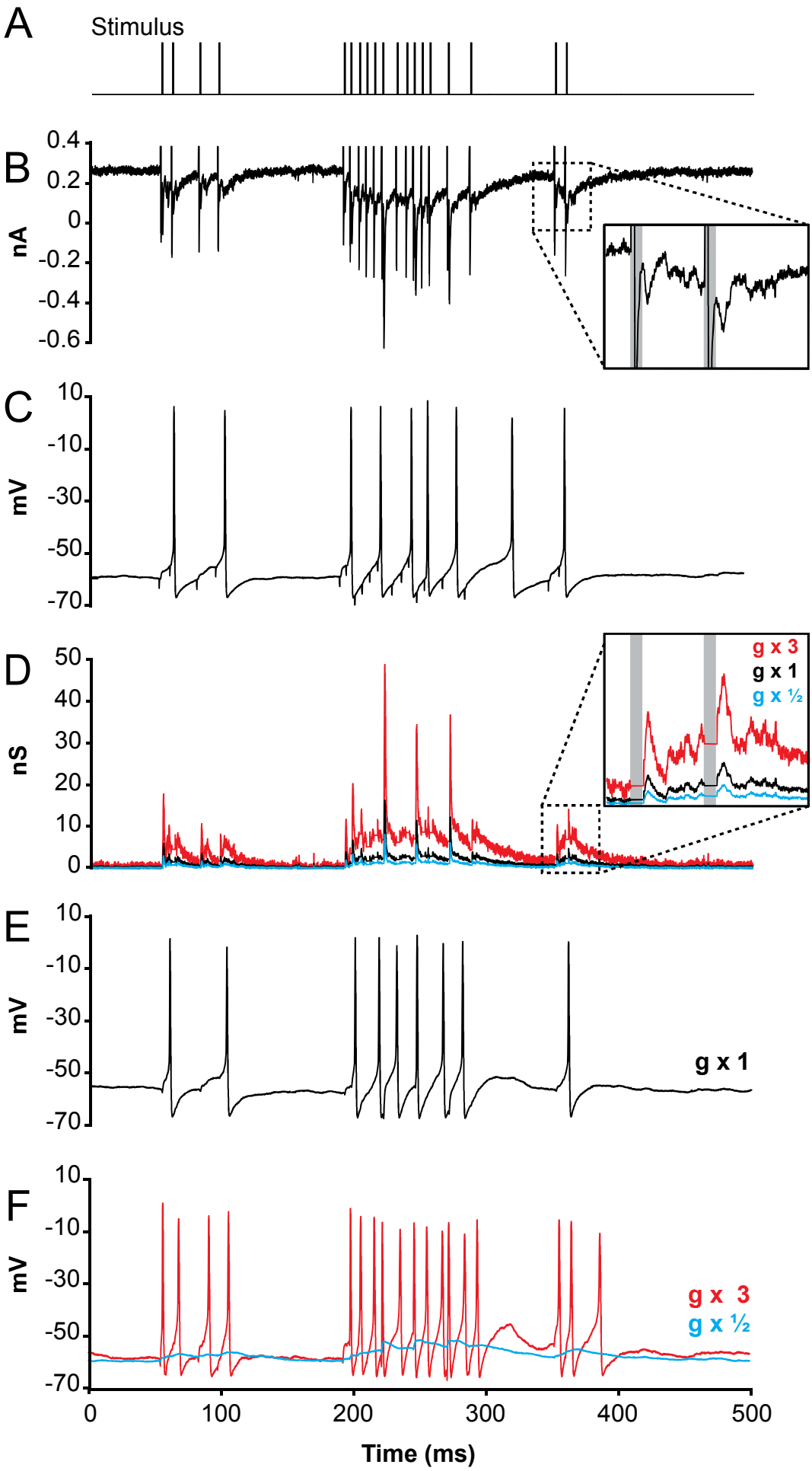
A
Stimulus
B
nA
0.4
0.2
0
-0.2
-0.4
-0.6
C
mV
10
-10
-30
-50
-70
D
nS
50
40
30
20
10
0
g x 3
g x 1
g x ½
E
mV
10
-10
-30
-50
-70
g x 1
F
mV
10
-10
-30
-50
-70
g x 3
g x ½
0
100
200
300
400
500
Time (ms)

Figure 2

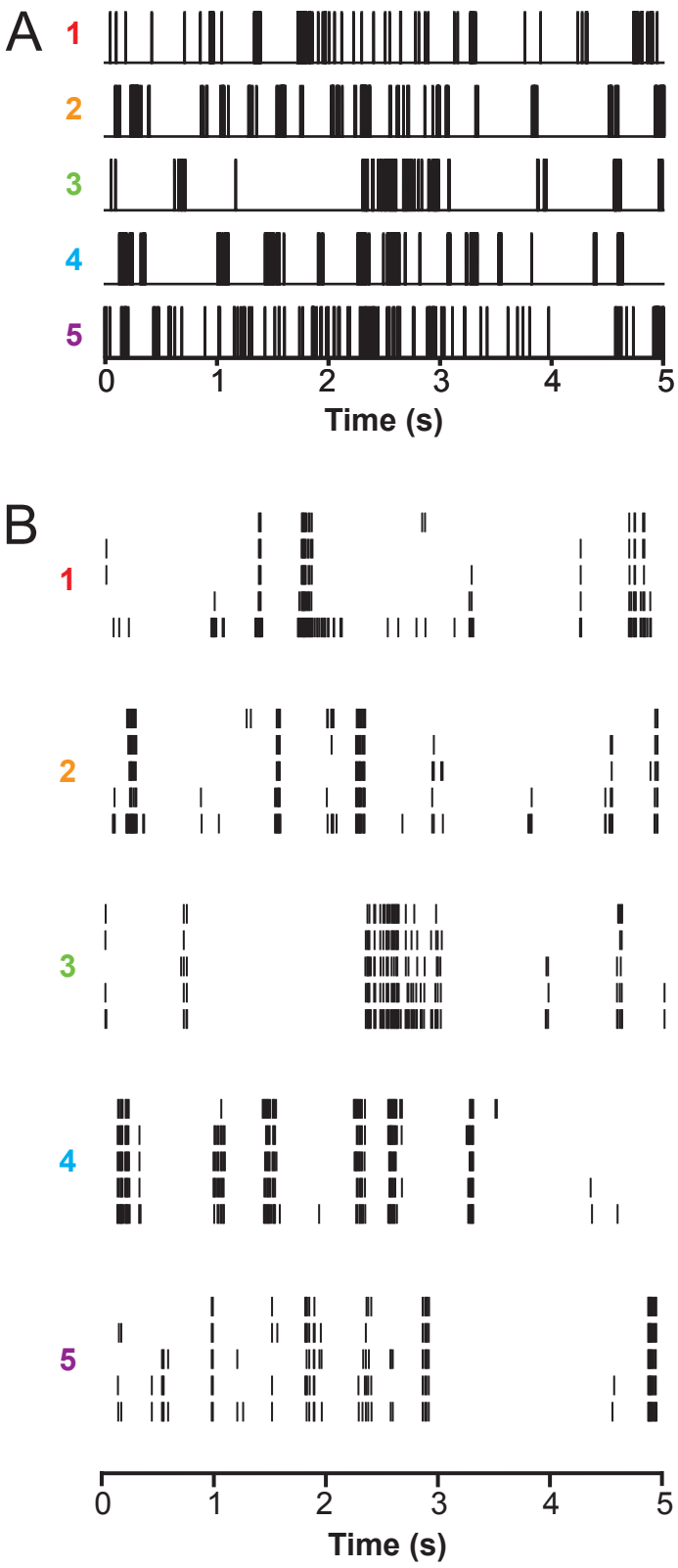
A
1
2
3
4
5
0
1
2
3
4
5
Time (s)
B
1
2
3
4
5
0
1
2
3
4
5
Time (s)

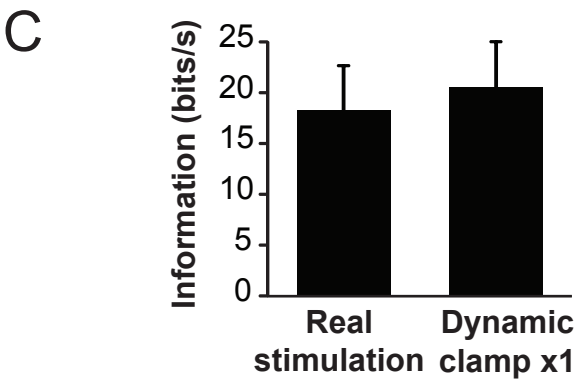
C
Information (bits/s)
25
20
15
10
5
0
Real stimulation
Dynamic clamp x1

Figure 3

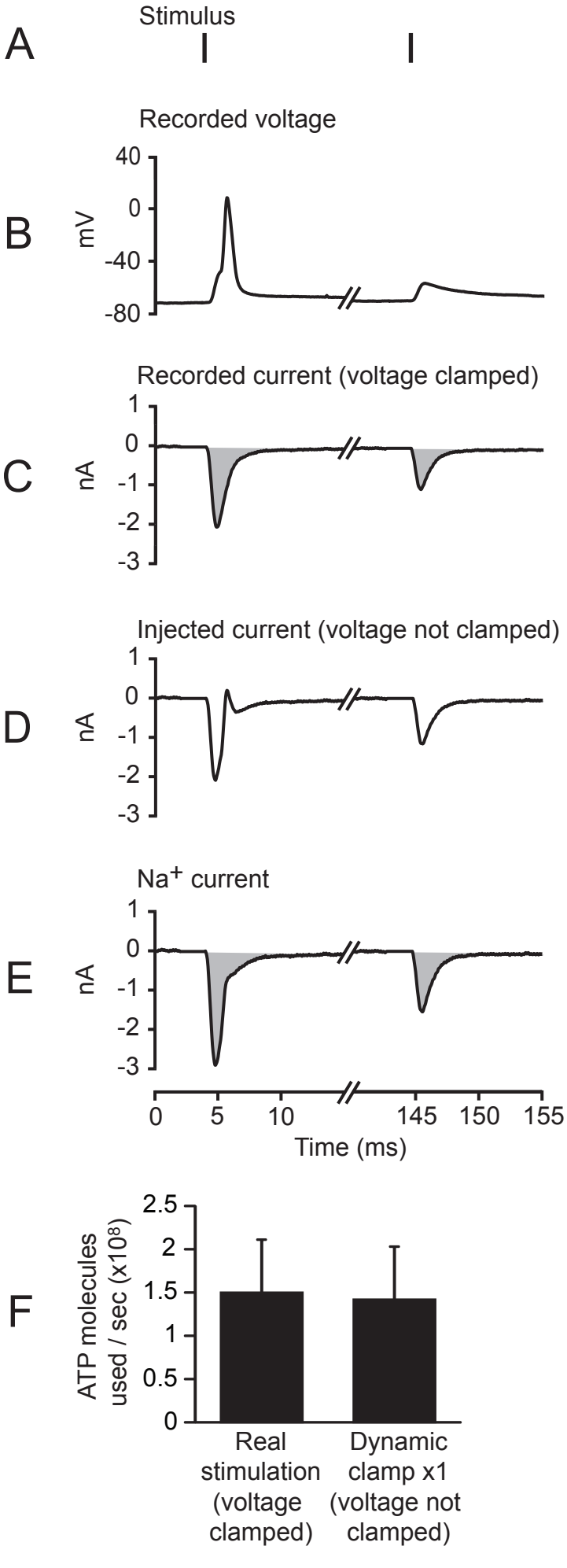
A
Stimulus
B
Recorded voltage
40
0
-40
-80
mV
C
Recorded current (voltage clamped)
1
0
-1
-2
-3
nA
D
Injected current (voltage not clamped)
1
0
-1
-2
-3
nA
E
Na+ current
1
0
-1
-2
-3
nA
0
5
10
145
150
155
Time (ms)
F
ATP molecules used / sec (x10^8)
2.5
2
1.5
1
0.5
0
Real stimulation (voltage clamped)
Dynamic clamp x1 (voltage not clamped)

Figure 4

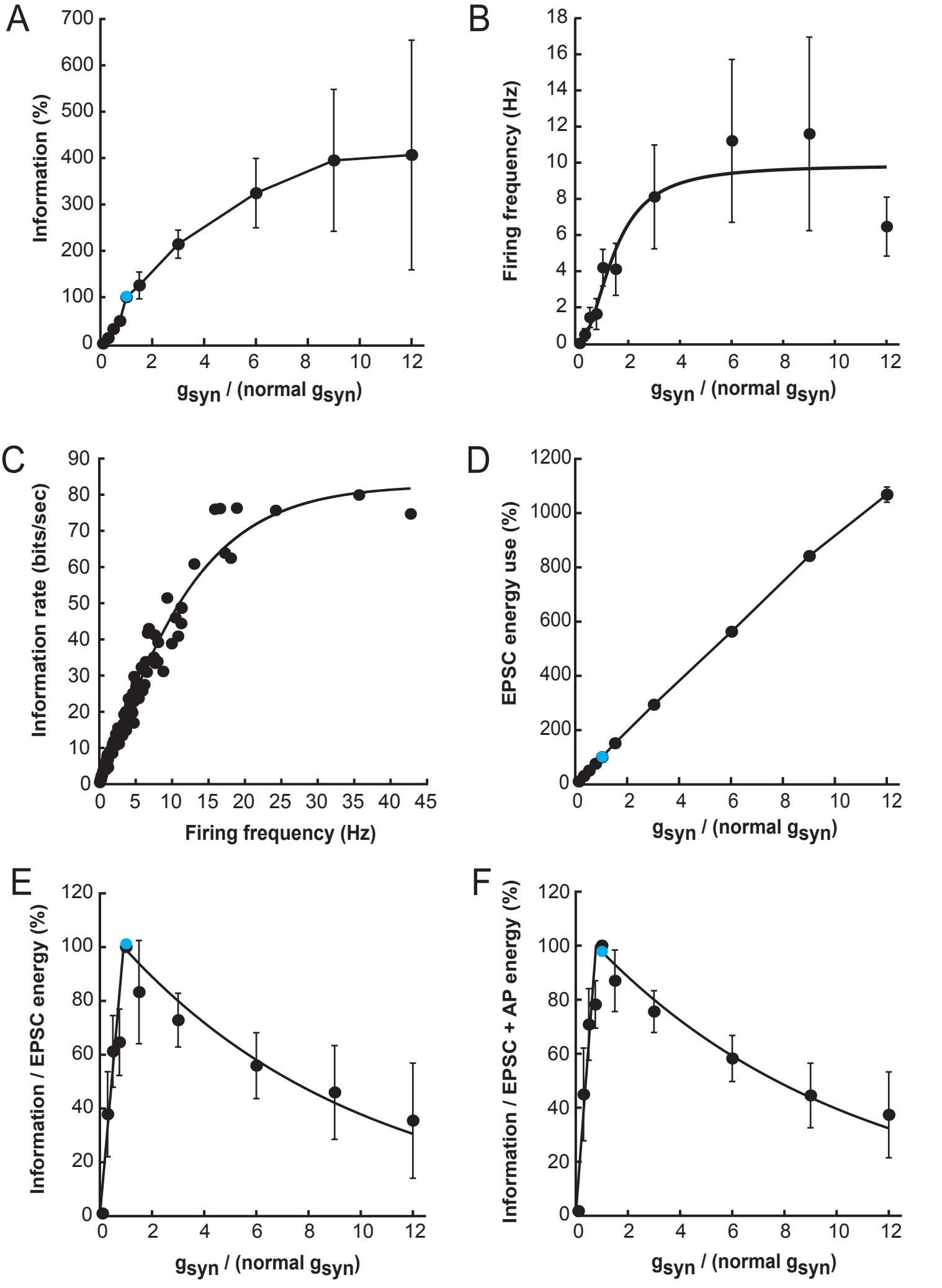
A
Information (%)
g_{syn} / (normal g_{syn})
B
Firing frequency (Hz)
g_{syn} / (normal g_{syn})
C
Information rate (bits/sec)
Firing frequency (Hz)
D
EPSC energy use (%)
g_{syn} / (normal g_{syn})
E
Information / EPSC energy (%)
g_{syn} / (normal g_{syn})
F
Information / EPSC + AP energy (%)
g_{syn} / (normal g_{syn})

Figure 5

Supplemental Information

Energy efficient information transfer by thalamic relay neurons

Julia J. Harris[*], Renaud Jolivet[*] and David Attwell

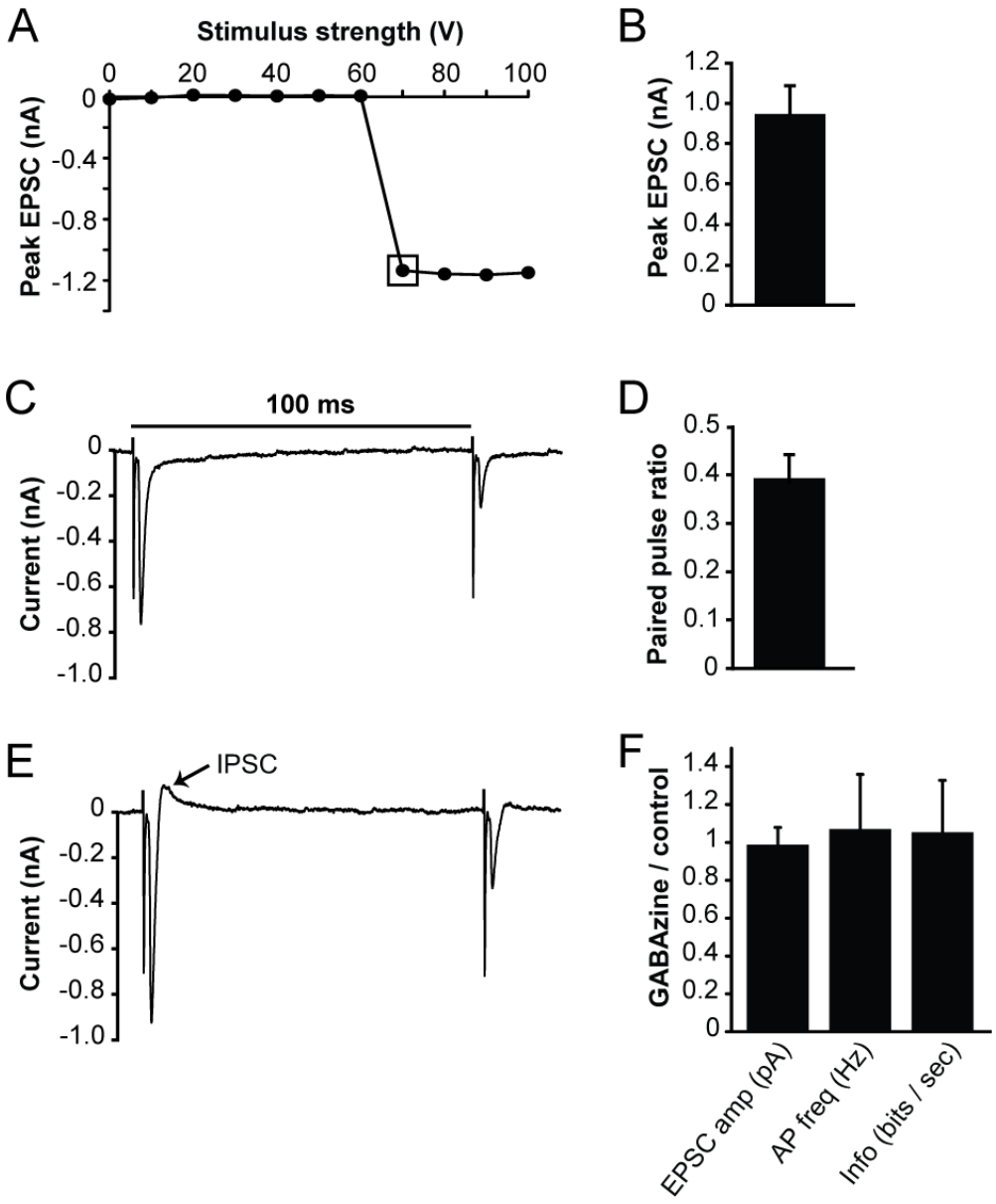

Figure S1 (related to Figure 1). Characterization of the optic tract input to dLGN cells. (A) Stimulus-response curve shows a single increase indicating stimulation of one axon. (B) Mean amplitude of first excitatory postsynaptic current (EPSC) in 18 cells. (C) Paired pulse depression of EPSC in a specimen cell evoked by stimuli 100 msec apart. (D) Mean paired pulse ratio (2^{nd} / 1^{st} EPSC) for 100 msec separation in 18 cells. (E) In the absence of GABAzine, some cells display disynaptic inhibition (seen as an IPSC after the EPSC), which tends to show postsynaptic depression (mean paired pulse ratio of IPSC = 0.6±0.2). (F) For the cells with disynaptic inhibition, GABAzine does not significantly alter the EPSC size ($p = 0.62$), the action potential frequency ($p = 0.69$) or the information rate ($p = 0.87$) of presynaptically stimulated LGN neurons (8 cells).

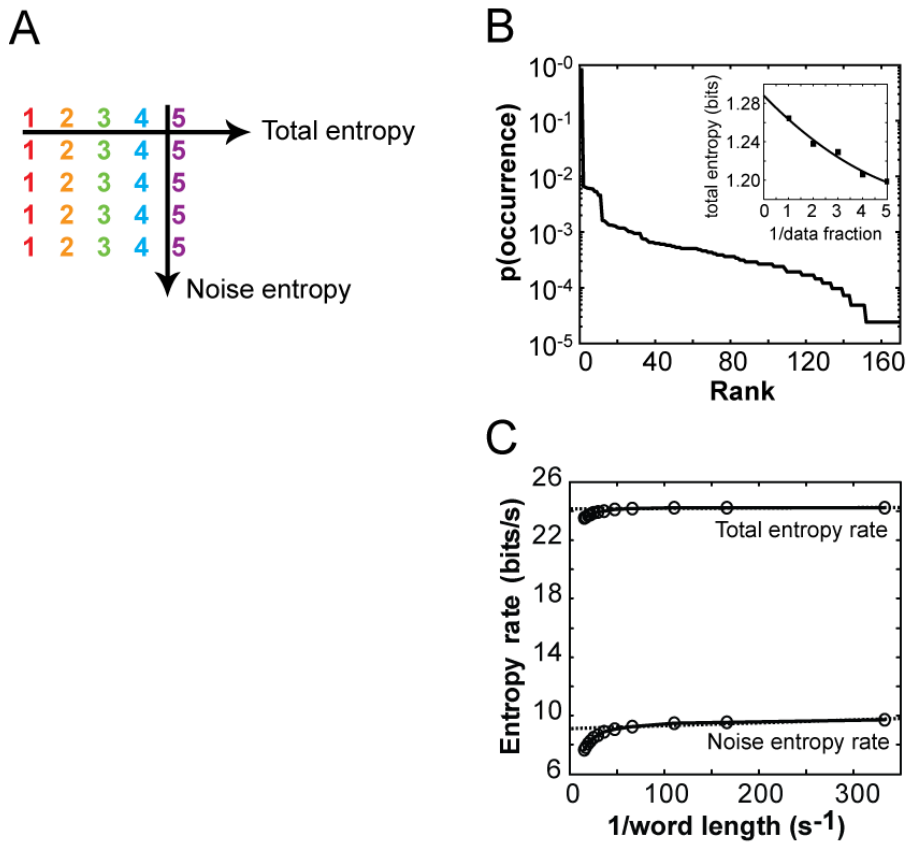

Figure S2 (related to Figure 3). Calculating mutual information. (A) Trains 1-5 were applied 5 times (in the order left to right, and then down the successive rows). Analysis of entropy across all 5 trains gives a measure of total response variability. Analysis of entropy across repeated application of the same train gives the noise entropy. (B) Probability of occurrence of each of the 10-letter words produced by application of all 5 trains for a specimen cell, ranked by probability value. Inset shows the dependence of the entropy, computed from this probability distribution according to the Shannon formula (Shannon, 1948) (see Experimental Procedures), on the fraction of data included in the analysis. Also plotted is a least squares fit of a quadratic function (see Experimental Procedures), where the intercept is our extrapolation to the true value of the entropy with infinite data (Strong et al., 1998). (C) Total and noise entropy for a specimen cell as a function of 1/word length (a word length of ten 3 msec bins corresponds to 1/word length = 33 sec^{-1}). Dashed lines indicate linear extrapolations to infinite word length (Strong et al., 1998).

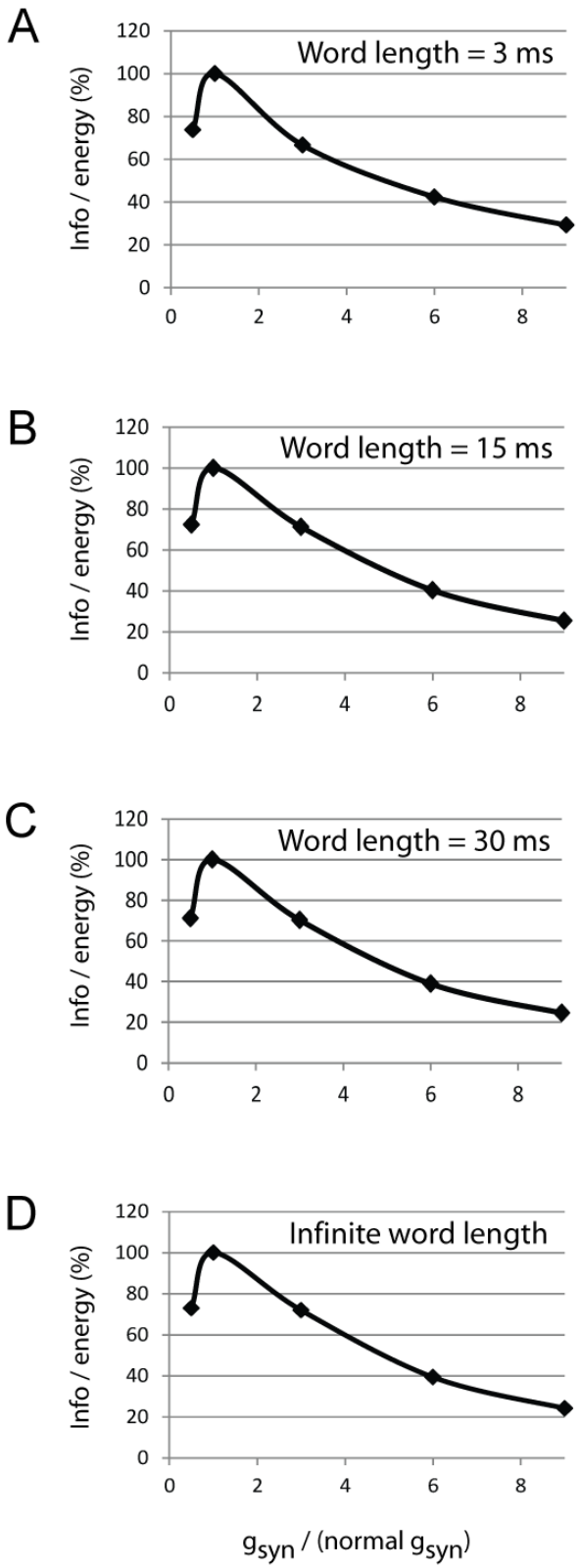

Figure S3 (related to Figure 5). Energetic efficiency calculation is independent of word length. Efficiency (bits transmitted / ATP used on EPSCs) plotted against synaptic conductance (altered using dynamic clamp to be 0.5, 1, 3, 6 and 9 times the biologically-occurring conductance) for an example cell. The relationship does not change when the information is calculated using words of length (A) 3 msec; (B) 15 msec; (C), 30 msec (used for all cells in Figure 5); or (D) linear extrapolation to infinite word length (as in Figure S2C). Bin size was always 3 msec. This analysis was performed on three cells, with similar results.

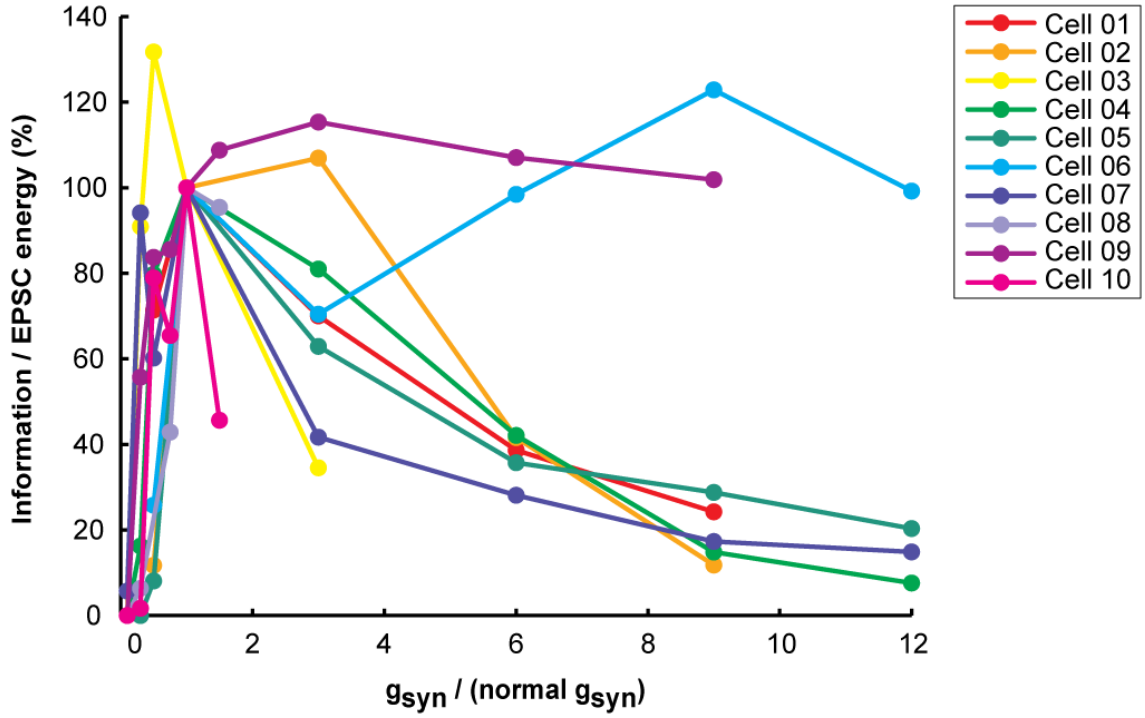

Figure S4 (related to Figure 5). Efficiency curves for individual cells. Efficiency (bits transmitted / ATP used on EPSCs) plotted against synaptic conductance (altered using dynamic clamp to be 0.1, 0.3, 0.5, 0.75, 1, 1.5, 3, 6, 9 or 12 times the biologically-occurring conductance) for each individual cell (not all conductance gains were performed on all cells). For each cell, the efficiency is normalised to the value at g_{syn}x1. Six out of ten cells show a maximum efficiency at the biological conductance value (g_{syn}x1), three cells show a maximum at a higher conductance magnitude (two at g_{syn}x3 and one at g_{syn}x9), and one cell shows a maximum at a lower conductance magnitude (at g_{syn}x0.5). Figure 5E is the average of these 10 curves.

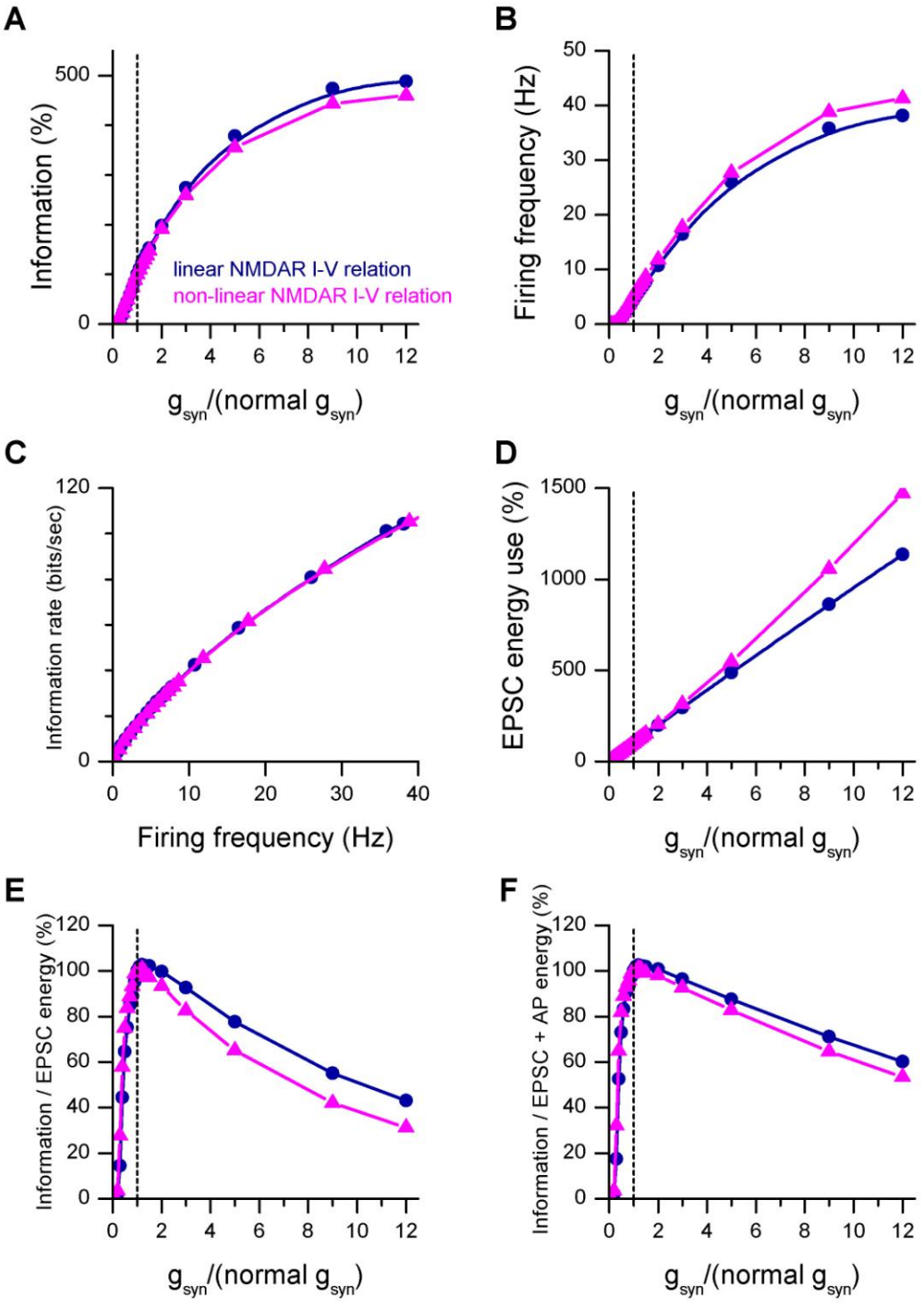

Figure S5 (related to Figure 5). Postsynaptic conductance magnitude maximises information transferred per energy used in a model of thalamic relay cells. (A) Dependence of the output information on synaptic conductance (g_{syn}) magnitude, when the thalamic relay cell model was stimulated with the AMPA and NMDA conductance recorded in response to experimental optic tract stimulation. The graph shows the effect of considering a linear NMDAR I-V relation (blue) or a non-linear NMDAR I-V relation (pink; see Supplemental Experimental Procedures). Information is normalized to the value with g_{syn} x1 for which the mean information rate was 21.4 bits/sec (linearized NMDA conductance) or 23.7 bits/sec (non-linear NMDA conductance). By comparison, the experimental information rate for recorded cells with presynaptic stimulation was 18.3±4.5 bits/sec.

Colours are the same in B to F. (B) Relationship between firing frequency and g_{syn} in the simulations. (C) Dependence of output information on mean output firing frequency evoked by stimulus trains with different g_{syn} values. Linearizing the NMDAR I-V relation had no significant effect on this relation. (D) Energy use on pumping out of postsynaptic ion influx as a function of g_{syn} multiplier. (E) Output information divided by energy use on reversing the ion influx generating postsynaptic currents in simulations shows a maximum close to the physiological value of g_{syn} (102.8% at g_{syn}=1.2 with the NMDAR I-V relation linearized and 100.8% at g_{syn}=1.2 with a non-linear NMDAR I-V relation). 100% (at g_{syn} = 1) corresponds to 31.9 bits per 10^8 ATP molecules used with the NMDAR I-V relation linearized and to 32.3 bits per 10^8 ATP molecules used with the non-linear NMDAR I-V relation, in the same range as the experimental value of 15.6±2.7 bits per 10^8 ATP molecules used. (F) Output information divided by energy use on reversing the ion influx generating postsynaptic currents and postsynaptic action potentials also shows a maximum close to the physiological value of g_{syn} (102.5% at g_{syn}=1.2 with the NMDAR I-V relation linearized and 101.1% at g_{syn}=1.2 with a non-linear NMDAR I-V relation). 100% (at g_{syn} = 1) corresponds to 8.0 bits per 10^8 ATP molecules used with the NMDAR I-V relation linearized and to 8.1 bits per 10^8 ATP molecules used with the non-linear NMDAR I-V relation, slightly below the experimental value of 9.0±1.2 bits per 10^8 ATP molecules used.

SUPPLEMENTAL EXPERIMENTAL PROCEDURES

Mathematical model of thalamic relay cells

The mathematical model of thalamic relay cells was adapted from earlier models (McCormick and Huguenard, 1992; Bazhenov et al., 1998a; Bazhenov et al., 1998b). Briefly, the model neuron consisted of a single compartment that included voltage-dependent currents described by Hodgkin-Huxley kinetics (Hodgkin and Huxley, 1952)

$$C_m \frac{dV}{dt} = -\sum_j i_j - i_{Hold} - i_{Syn}$$

where C_m = 1 μF/cm^2 is the membrane capacitance, V is the membrane voltage (in mV), i_{Hold} is the injected current, i_{Syn} is the synaptic current and i_j are the intrinsic currents. The cell surface area was $1.52 \cdot 10^{-4}$ cm^2, derived from the measured cell capacitance of 152±8 pF (mean±s.e.m., N=18) by assuming a specific capacitance of 1 μF/cm^2. All currents and conductances are subsequently reported per unit surface area (cm^2). Following Bazhenov and colleagues (Bazhenov et al., 1998a), the intrinsic currents included a leak current i_L, a potassium leak current i_{KL}, an A-type potassium current i_A, a T-type low threshold calcium current i_T, an h-current i_h, a fast sodium current i_{Na} and a fast potassium current i_K. All the intrinsic currents had the same general form

$$i = g m^M h^N (V - E)$$

where for each current i, g is the maximal conductance, $m(t)$ is the activation variable, $h(t)$ is the inactivation variable, E is the reversal potential and M and N are the number of independent activation and inactivation gates.

The i_h current was given by

$$i_h = g_{\max} O (V - E_h)$$

with E_h = –43 mV (Huguenard and McCormick, 1992). $g_{\max}$ = 0.0254 mS/cm^2 was set to match the average current recorded in our experiments in response to a 200 ms hyperpolarizing voltage-clamp pulse from –60 to –120 mV. The time dependence of the gating variable O was defined by

$$\frac{dO}{dt} = \frac{1}{\tau_O}(O_\infty - O)$$

with time constant $\tau_O = 1/\left[e^{(-14.59-0.086 \cdot V)} + e^{(-1.87+0.0701 \cdot V)}\right]$ (in msec) and steady-state variable $O_\infty = 1/\left[1 + e^{((V+75)/5.5)}\right]$ (Huguenard and McCormick, 1992).

The leak currents were given by

$$i_L = g_{\mathrm{L}}(V - E_L)$$

and

$$i_{KL} = g_{\mathrm{KL}}(V - E_K)$$

with E_L = –70 mV (McCormick and Huguenard, 1992). E_K was set to match the effective potassium reversal potential used in the experiments E_K = –105 mV, while g_L = 0.025 mS/cm^2 and g_{KL} = 0.025 mS/cm^2 were manually adjusted to match both the average input resistance at the resting membrane potential (R_i = 149±28 MΩ in experiments, mean ± s.e.m., N=18) and the resting membrane potential as recorded in experiments (V_{rest} = -76±2 mV in experiments, mean ± s.e.m., N=18; V_{rest} = –77.4 mV in the model).

The A-type potassium current was given by

$$i_A = g_A m^M h^N (V - E_K)$$

with M = 4 and N = 1. The time dependence for m and h was defined as for O, with

$$m_\infty = 1/\left[1 + e^{(-(V+60)/8.5)}\right]$$

$$\tau_m = 0.1 + 0.27/\left[e^{((V+35.8)/19.7)} + e^{(-(V+79.7)/12.7)}\right]$$

$$h_\infty = 1/\left[1 + e^{((V+78)/6)}\right]$$

and

$$\tau_h = 0.27/\left[e^{((V+46)/5)} + e^{(-(V+238)/37.5)}\right]$$

if V < –63 mV and $\tau_h = 5.1$ msec otherwise (Bazhenov et al., 1998a; Bazhenov et al., 1998b).

The T-type calcium current was given by

$$i_T = g_T m^M h^N (V - E_T)$$

with M = 2 and N = 1. The time dependence for m and h was defined as for O, with

$$m_\infty = 1/\left[1 + e^{(-(V+57)/6.2)}\right]$$

$$\tau_m = 0.13 + 0.22/\left[e^{(-(V+132)/16.7)} + e^{((V+16.8)/18.2)}\right]$$

$$h_\infty = 1/\left[1 + e^{((V+83)/4)}\right]$$

and

$$\tau_h = 8.2 + \left[56.6 + 0.27 \cdot e^{((V+115.2)/5)}\right]/\left[1 + e^{((V+86)/3.2)}\right]$$

E_T is given by $E_T = RT/2F \cdot \log(\mathrm{Ca}_0^{2+}/\mathrm{Ca}^{2+})$ with F = 96489 C/mol the Faraday constant, R = 8.314 J mol^{-1} K^{-1} the gas constant, T = 309 K the temperature and Ca_0^{2+} = 2 mM the extracellular calcium concentration. The intracellular calcium dynamics were defined by

$$\frac{d\mathrm{Ca}^{2+}}{dt} = -\frac{1}{\tau_{\mathrm{Ca}}}\left(\mathrm{Ca}^{2+} - \mathrm{Ca}_i^{2+}\right) - A\, i_T$$

with Ca_i^{2+} = 2.4·10^{-4} mM, the baseline intracellular calcium concentration, and A = 5.18·10^{-5} mM cm^2 msec^{-1} μA^{-1}, a constant.

The fast sodium current was defined by

$$i_{Na} = g_{Na} m^3 h (V - E_{Na})$$

with E_{Na} = +90 mV adapted to match the experiments. The maximal conductance g_{Na} = 4.4 mS/cm^2 was set to match the peak current recorded in experiments in response to a 200 ms +40 mV depolarizing voltage step from the resting membrane potential. The time dependence for *m* and *h* was defined by

$$\frac{dx}{dt} = \alpha_x (1 - x) - \beta_x x$$

where x stands for either *h* or *m* and with

$$\alpha_m = 0.32 \left[13.1 - V + V_{\text{shift}}^{\text{Na}}\right] / \left[e^{\left((13.1 - V + V_{\text{shift}}^{\text{Na}})/4\right)} - 1\right]$$

$$\beta_m = 0.28 \left[V - V_{\text{shift}}^{\text{Na}} - 40.1\right] / \left[e^{\left((V - V_{\text{shift}}^{\text{Na}} - 40.1)/5\right)} - 1\right]$$

$$\alpha_h = 0.128 \, e^{\left((17 - V + V_{\text{shift}}^{\text{Na}})/18\right)}$$

and

$$\beta_h = 4 / \left[1 + e^{\left((40 - V + V_{\text{shift}}^{\text{Na}})/5\right)}\right]$$

(Traub and Miles, 1991).

The fast potassium current was given by

$$i_K = g_K n^4 (V - E_K)$$

The maximal conductance g_K = 3.3 mS/cm^2 was set to match the steady-state current recorded in experiments in response to a 200 ms +40 mV depolarizing voltage step from the resting membrane potential. The time dependence for *n* was defined as for the sodium gating variables *m* and *h* with

$$\alpha_n = 0.032 \left[15 - V + V_{\text{shift}}^{\text{K}}\right] / \left[e^{\left((15 - V + V_{\text{shift}}^{K})/5\right)} - 1\right]$$

and

$$\beta_n = 0.5 \, e^{\left((10 - V + V_{\text{shift}}^{\text{K}})/40\right)}$$

(Traub and Miles, 1991).

$V_{\text{shift}}^{\text{Na}}$ = –60.1 mV and $V_{\text{shift}}^{\text{K}}$= –62.5 mV were manually adjusted to allow the model to be depolarized to –55 mV without spontaneously spiking. These values slightly differ from the values in the Traub and Miles model (1991) ($V_{\text{shift}}^{\text{Na}}$ = $V_{\text{shift}}^{\text{K}}$= –60 mV) and from the values in the model by Bazhenov and colleagues (1998a, 1998b) ($V_{\text{shift}}^{\text{Na}}$ = $V_{\text{shift}}^{\text{K}}$= –63 mV). i_{Hold} = -2.05 µA/cm^2 was set in subsequent simulations so as to hold the model at –55 mV. For a cell surface area of 1.52·10^{-4} cm^2, this corresponds to an injected current of ~310 pA, similar to experimentally measured values of 30-550 pA. g_A = 3 mS/cm^2 and g_T = 1.8 mS/cm^2 were set so that the model achieved an output frequency, when stimulated with the recorded synaptic conductance, similar to the average frequency observed in

experiments with extracellular stimulation (5.3 Hz in the model, 4.1±0.8 in the experiments, mean±s.e.m., N=18).

To determine the AMPA and NMDA synaptic conductance components generated by extracellular stimulation of retinal ganglion cells with the 125 second stimulus trains used in Figures 3 to 5, we recorded the evoked currents in thalamic relay neurons held at -55 mV with and without bath application of the NMDAR blocker 50 µM D-AP5 (in the presence of 5 µM GABAzine). Currents were converted to conductance by dividing them by the holding potential (i.e. using a reversal potential of 0 mV). To determine the time course of the NMDA component, the conductance time course recorded in AP5 was subtracted from the total conductance time course. This procedure was repeated with three cells and the average AMPA (g_{AMPA}) and NMDA (g_{NMDA}) conductance time courses that were evoked by the input stimulation trains were used as inputs in the simulations. To reproduce the experiments modulating the amplitude of the synaptic conductance, g_{AMPA} and g_{NMDA} were scaled by a gain factor varying between 0 and 12. Two batches of simulations were run, one with a linearized NMDA I-V relation, so that the total synaptic current varied linearly with voltage, as was used in the dynamic-clamp experiments, and one with a voltage-dependent NMDA conductance including Mg^{2+} block, to investigate whether our omission of this in the dynamic clamp experiments had a significant effect on the results. In the first case, the synaptic current i_{Syn} is simply given by

$$i_{Syn} = -(g_{AMPA} + g_{NMDA})\left(V - E_{\mathrm{excitatory}}\right)$$

with $E_{\mathrm{excitatory}}$ = 0 mV. To describe the NMDA non-linear I-V relation, we recorded the evoked currents in thalamic relay neurons generated by retinal ganglion cell stimulation during bath application of 1 µM NBQX (in the presence of 5 µM GABAzine) while holding the cell at different voltages (-74 mV to 36 mV in 10 mV steps). The recorded currents were then averaged across cells, and the voltage dependence was fitted by a function of the form $f(V) = a/(1 + b \cdot e^{-c \cdot V})$ with a, b and c as constants. i_{Syn} was then given by

$$i_{Syn} = -g_{\mathrm{AMPA}}\left(V - E_{\mathrm{excitatory}}\right) - g_{\mathrm{NMDA}}\left(\frac{9.69}{1 + 0.1688\, e^{-0.0717\, V}}\right)\left(V - E_{\mathrm{excitatory}}\right)$$

where $g_{\mathrm{AMPA}}(V\text{-}E_{\mathrm{excitatory}})$ and $g_{\mathrm{NMDA}}(V\text{-}E_{\mathrm{excitatory}})$ describe the time course of the separate synaptic current components at -55 mV.

To calculate information transfer at the simulated synapse, output spike trains were processed exactly as described for the experimental data.

To calculate the metabolic cost incurred by the modelled cell, for Fig. S5D i_{Syn} was integrated and converted to the corresponding ATP consumption per unit time, while for Fig. S5F the same procedure was followed for i_{Na}, i_h and i_T, and this was added to the ATP used on i_{Syn}. For i_h, the conductance was scaled by $(E_K - E_h)/(E_K - E_{Na})$ to isolate the contribution of sodium ions. For i_T, we assumed that each calcium ion is exchanged for 3 sodium ions (Attwell and Laughlin, 2001). For

i_{Syn}, the conductance was scaled by 7/13 (derived from the reversal potentials $E_{\text{excitatory}}$ = 0 mV, E_{Na} = +90 mV and E_K = -105 mV) to calculate the contribution of sodium ions.

To convert currents and conductance back and forth between absolute amplitudes (measured) and amplitudes scaled per unit surface, we used the average cell surface area taken from membrane capacitance measurements obtained in experiments ($1.52 \cdot 10^{-4}$ cm^2; see above). Simulations were run using custom-written MATLAB scripts (The Mathworks, Natick MA). Differential equations were integrated using the built-in solver *ode15s* with an integration time step dt = 0.05 ms.

SUPPLEMENTAL REFERENCES

Attwell, D. and Laughlin, S.B. (2001). An energy budget for signaling in the grey matter of the brain. JCBFM *21*, 1133-1145.

Bazhenov, M., Timofeev, I., Steriade, M. and Sejnowski, T.J. (1998a). Cellular and network models for intrathalamic augmenting responses during 10-hz stimulation. J. Neurophysiol. *79*, 2730-2748.

Bazhenov, M., Timofeev, I., Steriade, M. and Sejnowski, T.J. (1998b). Computational models of thalamocortical augmenting responses. J. Neurosci. *18*, 6444-6465.

Hodgkin, A.L. and Huxley, A.F. (1952). A quantitative description of membrane current and its application to conduction and excitation in nerve. J. Physiol.-London *117*, 500-544.

Huguenard, J.R. and McCormick, D.A. (1992). Simulation of the currents involved in rhythmic oscillations in thalamic relay neurons. J. Neurophysiol. *68*, 1373-1383.

McCormick, D.A. and Huguenard, J.R. (1992). A model of the electrophysiological properties of thalamocortical relay neurons. J. Neurophysiol. *68*, 1384-1400.

Traub, R.D. and Miles, D. (1991). Neuronal networks of the hippocampus (Cambridge: CUP).